Phase Space Reconstruction of a Particle Beam Using Elastic Scattering

Nils Hempelmann

September 15, 2014

Thesis submitted in partial fulfillment of the requirements for the degree Master of Science in Physics

Physics Institute III B

Faculty of Mathematics, Computer Science and Natural Sciences RWTH Aachen University

Thesis Supervisor: Prof. Dr. rer. nat. Jörg Pretz

Electric dipole moments in elementary particles would violate CP-symmetry and could lead to the discovery of CP-violation outside the Standard Model. The proposed measurement of the electric dipole moments of charged hadrons at storage rings such as the Cooler Synchrotron in Jülich would be very sensitive to systematic errors as the expected signals are extremely small. The experiments would measure the number of polarized particles scattered to the left and to the right of a fixed target and infer the electric dipole moment from the asymmetry in the rates. Such asymmetries can also be induced by a misalignment of the beam.

In this thesis, an algorithm to determine the transverse momentum and the position of incoming particles from elastic scattering events was developed and tested with Monte Carlo data from a simulation of a proposed polarimeter. As the measurement is performed event by event, it is possible to measure the statistical distribution of these variables, the phase space distribution of the transverse motion of particles in the storage ring. However, the reconstruction errors are in the same order of magnitude as the typical width of the distribution.

The phase space reconstruction uses a maximum likelihood fit. The likelihood function for the detector response is calculated numerically from a GEANT4 simulation. The fit can make use of the hit positions of the outgoing particle tracks and the energy they deposit in the detector.

The reconstruction achieves an event by event precision of about 5 mrad for the beam angle and about 200 μm for the beam position.

Contents

1 Introduction

The electric dipole moment (EDM) of elementary particles is a very sensitive indicator for the violation of charge parity symmetry (CP). The Standard Model of particle physics only predicts a small fraction of the CP-violation that is needed to account for the abundance of matter in the universe. By analyzing the cosmic microwave background, the COBE and WMAP experiments have measured the ratio of the net baryon number in the universe and the number of cosmic background photons [2]:

$$\eta = \frac{n_B - n_{\bar{B}}}{n_\gamma} = 6.1^{+0.3}_{-0.2} \cdot 10^{-10}.$$

This parameter describes how strongly matter dominated over antimatter in the early universe during baryogenesis, the formation of baryonic matter. The Standard Model prediction is only $\sim 10^{-18}$, which comes from the contribution of CP-violation in the weak interaction, which has been observed experimentally. This discrepancy is one of the most important unresolved problems in modern physics.

Like baryogenesis, an electric dipole moment in elementary particles is a violation of CP-symmetry. The value of the electric dipole moment could provide information on the extent and mechanism of CP-violation. All searches so far have only found upper limits and no signal.

Measurements of the electric dipole moment are based on spin precession in an electric or magnetic field. However, charged particles will be accelerated by the field and cannot be kept stationary. The dipole moment of charged particles like deuterons or protons could be measured in a storage ring [3].

Due to the small expected signal such experiments are very prone to systematic errors. All proposed experiments involve measuring the polarization of a beam at some point, which can be done by scattering the beam off a stationary target and calculating the asymmetry between particles scattered to the left and to the right hand side. Small asymmetries like this can also arise from uncertainties in the alignment of the beam and the detector.

The purpose of this thesis is to develop a method to accurately measure both the position and the direction of an incoming particle beam relative to the detector. This information can be used to correct for asymmetries introduced by misalignment, i.e. the beam entering the detector at an angle and position slightly different from the ideal beam axis. Elastic scattering events can be used to reconstruct the incident particle's original direction and position if both outgoing tracks are measured. The method is tested using Monte Carlo Data of deuteron-proton scattering at a kinetic energy of 236 MeV

measured with a proposed polarimeter consisting of two layers of silicon strip detectors. A similar reconstruction for a proton beam at higher energies was implemented at the Forschungszentrum Jülich [1].

2 Measurement of Electric Dipole Moments in Storage Rings

2.1 Fundamental Symmetries and the Electric Dipole Moment

Elementary particles can only have a nonzero electric dipole moment (henceforth abbreviated as EDM) if CP-symmetry is violated. The behavior of an EDM under parity and

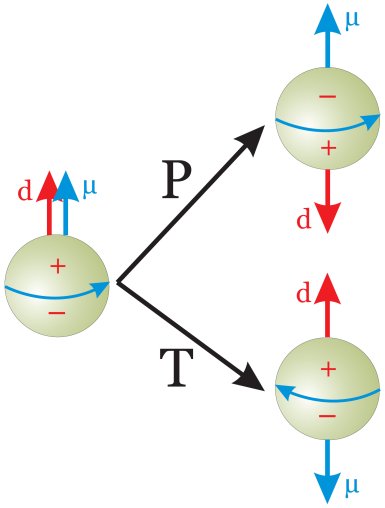

Figure 1: Behavior of the electric dipole moment under parity and time reversal transformation [4]. The magnetic dipole moment μ is even under parity transformation and odd under time reversal, while the electric dipole moment d is odd under parity and even under time reversal.

time reversal transformation is shown in fig. 1. As the magnetic dipole is proportional to the particle's spin, it transforms like an angular momentum: it is invariant under parity (P) but changes its sign under time reversal (T). The EDM can be thought of as the product of a position vector and an electric charge, which means it transforms like a position vector. The electric dipole moment changes its sign under parity but it is invariant under time reversal.

If a particle is to be symmetric under P- and T-transformations, either the EDM or the magnetic dipole moment of the particle must be zero. As the existence of magnetic dipole moments is a well-established fact, a nonzero EDM means that P- and T-symmetry is violated. According to the CPT-theorem, all particles must be symmetrical under a combination of charge conjugation, time reversal and parity transformation. This means that CP-symmetry must be violated as well.

There are two CP-violating terms in the Standard Model. The first is the CP-violating phase in the Cabibbo-Kobayashi-Maskawa matrix, which describes quark flavor mixing. It leads to CP-violation in the weak interaction. The second CP-violating term is the θ term in quantum chromodynamics. The CP-violating phase θ could in principle have any value from 0 to 2π, but the measurements of hadronic EDMs limit θ to about 10^{-10}, which seems unnaturally small. The question why the strong interaction is CP-symmetric is called the strong CP problem and is not yet resolved.

The known CP-violating effects in the Standard Model lead to an EDM of around 10^{-32} to $10^{-31}\,e\,\mathrm{cm}$, which is below the expected sensitivity of planned experiments of around $10^{-29}\,e\,\mathrm{cm}$. Extensions of the Standard Model such as supersymmetric models predict higher EDMs that might be measurable.

2.2 Electric Dipole Measurement of Charged Hadrons in Storage Rings

The EDM of charged hadrons could be measured in experiments with storage rings [3]. All EDM measurements are based on the precession of electric dipoles in an electric or magnetic field. The EDM must be parallel or antiparallel to the spin vector because

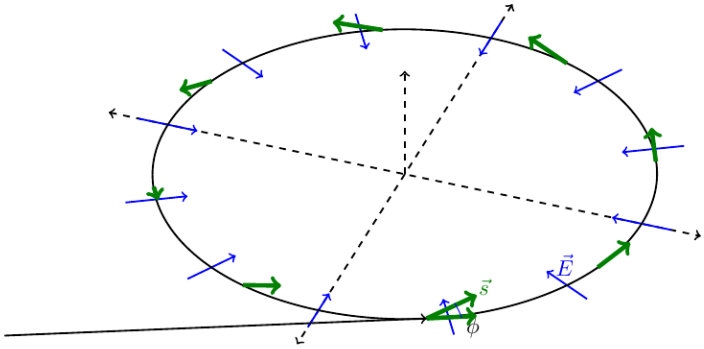

Figure 2: Basic layout of an EDM measurement in an electric storage ring [3]. A beam of longitudinally polarized particles is injected into the ring. The polarization rotates as the EDM interacts with the radial electric field. The vertical polarization can be measured with a suitable detector.

the particle has no other property that could single out a direction. The motion of the spin vector $\mathbf{S}$ follows the differential equation

$$\frac{d\mathbf{S}}{dt} = \boldsymbol{d} \times \mathbf{E}^*. \tag{2.1}$$

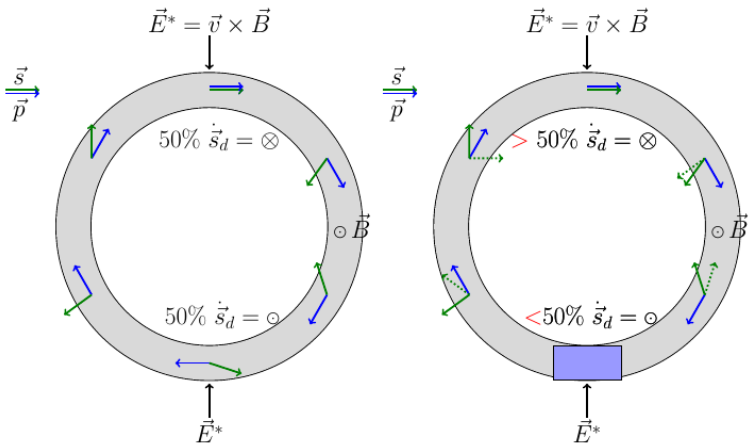

Figure 3: EDM measurement using a magnetic ring [3]. In the particle's rest frame, there is an electric field pointing radially inward that tilts the spin. The spin moves upwards when the spin vector is parallel to the momentum vector and downwards when the spin is antiparallel to the momentum. This would result in an oscillating motion as both situations occur over half of the orbit and compensate each other (left). A Wien filter will not affect the particles trajectory, but it perturbs the spin. This way the spin will move in one direction more than in the other, facilitating polarization build-up if the Wien filter is operated at the correct frequency (right).

Where $\mathbf{d}$ is the EDM vector and $\mathbf{E}^*$ is the electric field in the rest frame of the particle.

In the proposed experiments, a longitudinally polarized particle beam is injected into a storage ring. The EDM will tilt the spin axis as described by (2.1). This leads to a gradual build up of vertical polarization that can be measured with a suitable detector (see section 3.3).

Different storage ring concepts have been proposed to measure the EDM. The ring can either use only an electric field to guide the particle and rotate the beam polarization, as shown in fig. 1, a combination of electric and magnetic fields or a ring that only uses a magnetic field (fig. 3). The last concept requires a Wien filter to build up vertical polarization .

2.3 Polarized Beams in Nuclear Reactions

The polarization of a particle beam can be measured using a reaction whose cross section depends on the spin orientation. The dependency of the cross section on the spin orientation is described by the so called analyzing power. One has to distinguish between spin-1 particles like deuterons and spin-1/2 particles like protons.

A spin-1/2 particle can be described by a Pauli spinor with two complex-valued components. There are three operators, the Pauli matrices σ_i, that describe the spin component in the direction of each Cartesian coordinate. A particle beam can be treated as a statistical ensemble of many spin-1/2 particles. The statistical averages of the spins in each direction form a classical vector:

$$\mathbf{P} = \begin{pmatrix} P_1 \\ P_2 \\ P_3 \end{pmatrix} = \frac{\hbar}{2} \begin{pmatrix} \langle \sigma_1 \rangle \\ \langle \sigma_2 \rangle \\ \langle \sigma_3 \rangle \end{pmatrix}. \tag{2.2}$$

The pointed braces ("$\langle \ldots \rangle$") denote a statistical average over the ensemble rather than a quantum mechanical expectation value for a pure state. This vector is equivalent to the density matrix of the polarization states in the beam [5, chapter 1].

$$\rho = \frac{1}{2} \left(I + P_1 \sigma_1 + P_2 \sigma_2 + P_3 \sigma_3 \right), \tag{2.3}$$

where I is the 2×2 identity matrix.

For a spin-1 particle, the situation is more complicated. Having three spin eigenstates, the particle can be described by a three component spinor. The spin operator also becomes a three by three matrix, but retains the same algebra as for the spin-1/2 case. The polarization of a beam of spin-1 particles cannot be represented completely by a

vector of three components. As the spin has three eigenstates, the density matrix has $3^2 - 1$ degrees of freedom, corresponding to three times three entries minus one degree of freedom because the trace must be one. Three of those are fixed by the expectation values of the spin operators $P_i = \langle S_i \rangle$, where S_i is the spin-1 operator. As in the spin-1/2 case they form a classical vector called the vector polarization. The remaining five degrees of freedom form a symmetric tensor of rank two, $P_{ij} = \langle S_{ij} \rangle$ with

$$S_{ij} = \frac{3}{2}\left(S_i S_j + S_j S_i\right) - 2I\delta_{ij} \tag{2.4}$$

In analogy to eq. 2.3 this can be used to represent the beam's density matrix [5, chapter1]:

$$\rho = \frac{1}{3}\left(I + \frac{3}{2}\sum_{i=1}^{3} P_i S_i + \frac{1}{3}\sum_{i,j=1}^{3} P_{ij} S_{ij}\right), \tag{2.5}$$

where I is the 3×3 identity matrix. In the particle reactions used for polarimetry, the spin dependence of the cross section induces and azimuthal asymmetry. For spin-1/2 particles, the differential cross section for an unpolarized target is [5, chapter 3]:

$$\frac{d\sigma}{d\Omega}(\theta, \phi) = \frac{d\sigma_0}{d\Omega}(\theta) \cdot \left(1 + \mathbf{A}(\theta) \cdot \mathbf{P}\right). \tag{2.6}$$

$\mathbf{A}$ is a vector called the analyzing power, which depends on the reaction and the scattering angle. σ_0 is the cross section for the same reaction if the beam is unpolarized.

For spin-1 particles, the cross section is:

$$\frac{d\sigma}{d\Omega}(\theta, \phi) = \frac{d\sigma_0}{d\Omega}(\theta) \cdot \left(1 + \frac{3}{2}\mathbf{A} \cdot \mathbf{S} + \frac{1}{3}\sum_{i,j=1}^{3} S_{ij} A_{ij}\right). \tag{2.7}$$

Here $\mathbf{A}$ is again the vector analyzing power and A_{ij} is the tensor analyzing power. Assuming conservation of parity, a vector polarization pointing upwards and no tensor polarization in the case of spin-1 particles, 2.3 and 2.7 can be further simplified to

$$\frac{d\sigma}{d\Omega}(\theta, \phi) = \frac{d\sigma_0}{d\Omega}(\theta) \cdot \left(1 + A_2(\theta) \cdot P_2 \cdot \cos\phi\right) \tag{2.8}$$

$$\frac{d\sigma}{d\Omega}(\theta, \phi) = \frac{d\sigma_0}{d\Omega}(\theta) \cdot \left(1 + \frac{3}{2} A_2(\theta) \cdot S_2 \cdot \cos\phi\right). \tag{2.9}$$

The former formula describes the spin-1/2 case, the latter the spin-1 case. The vector components labeled with the index 2 are defined to point upwards in the laboratory frame. ϕ is the azimuth angle of the outgoing particle.

2.4 Systematic Errors and Beam Misalignment

A polarimeter measures the the angular distribution of the outgoing particles; a deviation from a radially symmetric distribution indicates that the beam is polarized. In the simplest setup, a polarimeter consists of two identical particle detectors, one to the right of the beam ($\phi = \pi$) and one to the left ($\phi = 0$). The polarization is calculated from the count rates of both detectors. However an asymmetry can also be induced by slight differences in the detector acceptance or a beam that enters the detector at a wrong angle or at the wrong position. These effects can be mitigated by constructing ratios of measured event rates to cancel out systematic uncertainties [7, 6]. In this section, the influence of of these geometrical effects will be examined following the calculations in [6]

When measuring the polarization of a deuteron beam with a quantization axis perpendicular to the beam direction the cross section from (2.9) can be stated as:

$$\sigma = \sigma_0 \left(1 + pA\right). \tag{2.10}$$

$p = \sqrt{3} \cdot (f_1 - f_{-1}) \cos\phi$ is the vector polarization defined using the fractions of particles in the spin up and spin down states (f_1, f_{-1}). $A = A_2$ is the vector analyzing power; the index 2 is suppressed for clarity. σ is still the differential cross section previously written $\frac{d\sigma}{d\Omega}$. The derivative notation will be used for Taylor expansions in this section.

If the beam enters the detector at an angle $\Delta\theta$ that is defined as positive if the beam is inclined towards the right detector, the unpolarized cross section can be approximated as

$$\sigma_0 \left(\Delta\theta\right) = \sigma_0 \left(0\right) + \frac{\partial \sigma_0}{\partial \theta} \Delta\theta + \frac{1}{2} \frac{\partial^2 \sigma_0}{\partial \theta^2} \left(\Delta\theta\right)^2 + \mathcal{O}\left(\left(\Delta\theta\right)^3\right). \tag{2.11}$$

The analyzing power is

$$A \left(\Delta\theta\right) = A \left(0\right) + \frac{\partial A}{\partial \theta} \Delta\theta + \frac{1}{2} \frac{\partial^2 A}{\partial \theta^2} \left(\Delta\theta\right)^2 + \mathcal{O}\left(\left(\Delta\theta\right)^3\right). \tag{2.12}$$

As the polarimeter detectors cover a large solid angle, the cross sections and analyzing powers are averages over the detector acceptance. They depend on both the particle reaction used and the detector setup. Errors from the beam position can be treated in a similar way. At forward scattering angles, the angle θ and the position x are connected

over the formula $x = \theta R$, where R is a parameter for the effective distance between the target and the detector.

The simplest method to measure the polarization is the left-right asymmetry

$$\epsilon = \frac{\sigma_L - \sigma_R}{\sigma_L + \sigma_R} \tag{2.13}$$

σ_L and σ_R are the cross sections for the left and the right detector. Inserting the formula for the cross section and the expansion for the dependency on $\Delta\theta$ yields

$$\begin{aligned} \epsilon(\Delta\theta) &= \epsilon(0) + \left[\frac{1}{\sigma}\frac{\partial\sigma}{\partial\theta} - \epsilon^2\left(\frac{1}{\sigma}\frac{\partial\sigma}{\partial\theta} + \frac{1}{A}\frac{\partial A}{\partial\theta}\right)\right]\Delta\theta \\ &+ \left\{\epsilon\left[\frac{1}{2A}\frac{\partial^2 A}{\partial\theta^2} - \left(\frac{1}{\sigma}\frac{\partial\sigma}{\partial\theta}\right)^2\right] + \epsilon^3\left(\frac{1}{\sigma}\frac{\partial\sigma}{\partial\theta} + \frac{1}{A}\frac{\partial A}{\partial\theta}\right)^2\right\}(\Delta\theta)^2 \end{aligned} \tag{2.14}$$

Both first and second order corrections appear for the asymmetry.

The first order term can be avoided by using the so called cross ratio method [7, 6]. Two measurements of the counting rate are taken using opposite vector polarization of the beam (+, −). The asymmetry is

$$\epsilon_{CR} = \frac{r-1}{r+1}$$

with

$$r^2 = \frac{\sigma_{L,+}\cdot\sigma_{R,-}}{\sigma_{L,-}\cdot\sigma_{R,+}}. \tag{2.15}$$

The ratio in eq. 2.15 is constructed to make asymmetries between the detectors cancel. Another error parameter u is introduced to model the difference of the positive and the negative polarization. Using the definition from (2.10), the positive polarization is $p_+ = u + p$ and the negative polarization is $p_- = u + p$. The Taylor expansion in the errors is

$$\begin{aligned} \epsilon_{CR}(\Delta\theta) &= \epsilon_{CR}(0) + \frac{\epsilon^2}{1-\epsilon^2}u^2 - \frac{2\epsilon^2}{1-\epsilon^2}\frac{1}{A}\frac{\partial A}{\partial\theta}u(\Delta\theta) \\ &+ \left[\frac{\epsilon}{2}\frac{1}{A}\frac{\partial^2 A}{\partial\theta^2} - \frac{\epsilon^2}{1-\epsilon^2}\left(\frac{1}{A}\frac{\partial A}{\partial\theta}\right)^2\right](\Delta\theta)^2 \end{aligned} \tag{2.16}$$

All first order terms and all derivatives of the cross section disappear, which makes the cross ratio method preferable to the left-right asymmetry method. More schemes

for measuring the asymmetry exist, some of which also use a measurement with an unpolarized beam as a reference point.

2.5 The Cooler Synchrotron (COSY)

The Cooler Synchrotron [8, 9] is a storage ring for protons and deuterons at the Forschungszentrum Jülich. It has a circumference of 184 m and accelerates particles to momenta between 0.3 and 3.4 GeV/c. Fig. 4 shows an overview of COSY and the experiments

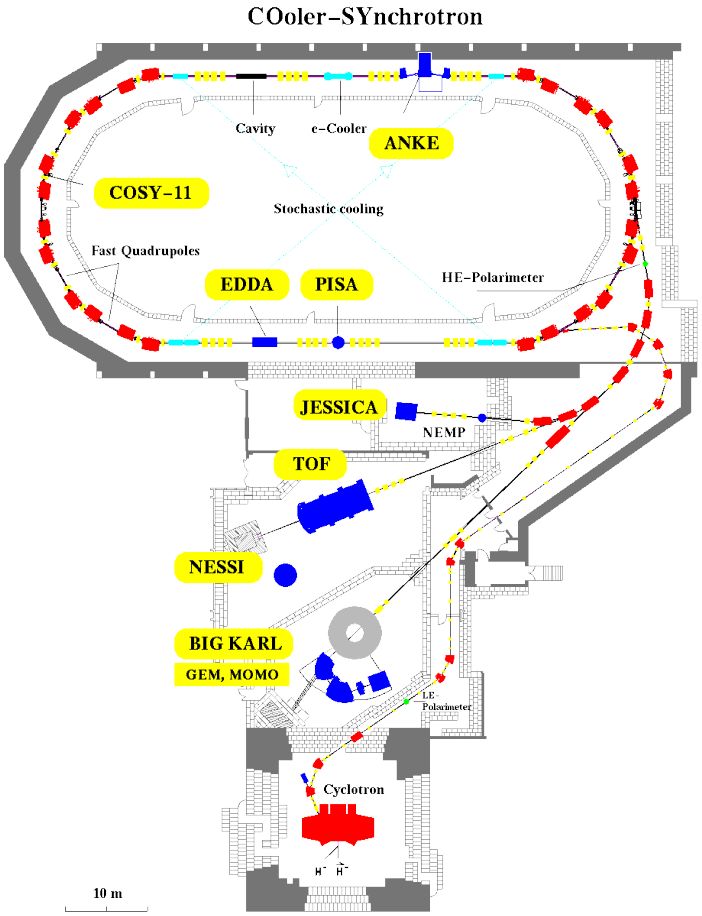

Figure 4: Overview of the Cooler Synchrotron (COSY)

performed using the storage ring. The accelerator can be operated with a polarized or an unpolarized beam. COSY can heat or cool the beam to control the beam phase space. A beam with a momentum of up to 600 MeV can be cooled using the electron cooler, above 1.5 MeV the stochastic cooler can be used. Heating the beam works by applying a high frequency electic field perpendicular to the beam to induce a transverse motion.

COSY is being used for precursor experiments to measure the electric dipole moment of charged hadrons. The purely magnetic ring method described in section 2.2 could be implemented on a relatively short timescale [3].

3 Beam Reconstruction

3.1 Beam Phase Space

In a storage ring, charged particles move along a more or less circular orbit. The centripetal force is provided by dipole magnets. For an ideal particle, the orbit is closed and constant over time. A real accelerator is always filled with a number of particles that have slightly different trajectories. The particles have some transverse momentum perpendicular to the ideal orbit, their positions spread to both sides as well.

For an electric dipole moment measurement, the important figures are the particle's position and momentum as it enters the detector. In an ideal beam all particles would have the same momentum

$$\mathbf{p}_{ideal} = \begin{pmatrix} 0 \\ 0 \\ 1 \end{pmatrix} p.$$

The coordinate system is defined in the laboratory rest frame. The z-axis is the central axis of the detector and matches the ideal beam direction. The y-axis points upwards and the x-axis to the left forming a right-handed coordinate system. In real accelerators, the orbit of each particle is slightly different from the ideal. The transverse momentum is nonzero and the longitudinal momentum may also deviate from the ideal value. The momentum of a real particle is:

$$\mathbf{p}_{real} = \begin{pmatrix} x' \\ y' \\ \sqrt{1 - x'^2 - y'^2} \end{pmatrix} p, \tag{3.1}$$

where x' and y' are small dimensionless parameters. They are defined as the ratio between the transverse momentum along either axis and the total momentum. For small values, they are approximately equal to the angle between the z-axis and the beam direction projected onto the plane defined by the z-axis and the x- or the y-axis.

The magnitude of the momentum is treated as constant because it is known to a very good precision ($\delta p/p \sim 2 \cdot 10^{-4}$) and because it is of lesser importance to the systematic uncertainties in EDM measurements. A beam that enters the polarimeter at a nonzero inclination induces an asymmetry between the left and right detector whereas a beam that has a slightly different energy than expected will only change the cross sections and analyzing powers symmetrically for both sides. Additionally, leaving the magnitude as a free parameter can lead to a degeneracy of the maximum likelihood fit (section 4). The

number of parameters would equal the number of independent measured variables, which leaves no degrees of freedom.

The position of a particle can be described by two additional parameters x and y that denote the particle track's distance to the z-axis along the x- and the y-axis, respectively. In total, it takes four parameters to fully describe a non-ideal particle trajectory. This corresponds to the six degrees of freedom of a point mass minus one for fixing the magnitude of the momentum and minus one for only determining a line along which the particle moves rather than its precise position on that line.

These parameters also fix a point in the phase space of the transverse motion of a particle in the beam, its position and transverse momentum. As the beam is focused by external conservative forces, the phase space volume of the beam must remain constant (Liouville's theorem). In the context of particle accelerators that phase space volume is called the emittance; it has the dimension angle times distance or mm × mrad.

The aim of this thesis is to develop a method to measure the distribution of particles in phase space using a detector that also serves as the polarimeter. The averages of the position and momentum distributions can be used to correct for the systematic uncertainties described in section 2.4. The event by event distribution might also be used to measure the quality and focusing point of the beam and help in calibration.

3.2 Elastic Scattering

Elastic scattering is a type of scattering in which no kinetic energy is converted to other forms of energy, i.e. the outgoing particles are of the same type as the ingoing particles. The kinematics of these events can be derived using the conservation of four momentum in special relativity. In this thesis, elastic scattering is used to reconstruct the momentum and position of particles in a beam by measuring the outgoing tracks and calculating the incident particle momentum using kinematic relations.

This section deals with the kinematics of elastic scattering off a fixed target. Throughout sections 3 and 4 the outgoing beam particle will be referred to as the ejectile. The outgoing particle that was at rest before scattering will be referred to as the recoil. In case of elastic deuteron-proton scattering the ejectile is a deuteron and the recoil is a proton. The formalism is applicable to other reactions as well. The fact that the target is initially at rest simplifies the kinematics. Given the scattering angle in the center of mass frame θ_{cm}, the momenta in the laboratory frame can be calculated using the following formulas [10]:

$$p_{\mathrm{ej}} \cos\left(\theta_{\mathrm{ej}}\right) = -p_{\mathrm{cm}} \cos\left(\theta_{\mathrm{cm}}\right) \cosh\left(\chi\right) + \sqrt{p_{\mathrm{cm}}^2 + m_{\mathrm{proj}}^2} \sinh\left(\chi\right) \tag{3.2}$$

$$p_{\mathrm{ej}} \sin\left(\theta_{\mathrm{ej}}\right) = p_{\mathrm{cm}} \sin\left(\theta_{\mathrm{cm}}\right) \tag{3.3}$$

$$p_{\mathrm{rec}} \cos\left(\theta_{\mathrm{rec}}\right) = p_{\mathrm{cm}} \cos\left(\theta_{\mathrm{cm}}\right) \cosh\left(\chi\right) + \sqrt{p_{\mathrm{cm}}^2 + m_{\mathrm{tar}}^2} \sinh\left(\chi\right) \tag{3.4}$$

$$p_{\mathrm{rec}} \sin\left(\theta_{\mathrm{rec}}\right) = p_{\mathrm{cm}} \sin\left(\theta_{\mathrm{cm}}\right). \tag{3.5}$$

Where θ_{ej} and θ_{rec} are the scattering angles of ejectile and recoil in the laboratory frame, p_{ej} and p_{rec} are the magnitudes of the respective momenta and m_{proj} and m_{tar} are the masses of the projectile and the target particles. p_{cm} is the particles' momentum in the center of mass frame:

$$p_{\mathrm{cm}} = \sqrt{\frac{\left(s - m_{\mathrm{proj}}^2 - m_{\mathrm{tar}}^2\right)^2 - 4 m_{\mathrm{proj}}^2 m_{\mathrm{tar}}^2}{4s}}. \tag{3.6}$$

With the Mandelstam variable s defined as

$$s = \left(m_{\mathrm{tar}} + m_{\mathrm{proj}}\right)^2 + 2 m_{\mathrm{tar}} E_{\mathrm{kin}}, \tag{3.7}$$

where E_{kin} is the kinetic energy of the projectile. The rapidity χ is

$$\chi = \log\left(\frac{p_{\mathrm{cm}} + \sqrt{m_{\mathrm{tar}}^2 + p_{\mathrm{cm}}^2}}{m_{\mathrm{tar}}}\right). \tag{3.8}$$

The momenta of the ingoing and outgoing particles are coplanar. To describe the scattering event completely, an additional azimuth angle ϕ_{scat} is required. ϕ_{scat} is defined as the azimuth angle of the ejectile track.

3.3 Polarimeter Concept and Measurement of Tracks

The beam phase space reconstruction is performed using Monte Carlo data from a simulation of a possible future polarimeter [11]. The simulation is based on the GEANT4 software package [13]. The polarimeter is shown in fig. 5. Its main components are a fiber tracker endcap and a barrel section consisting of two layers of silicon strip detectors. The barrel section fits inside the beam tube to measure the particles without any multiple scattering or ionization in the tube. The inner silicon layer lies at a distance of 30.1 mm from the beam axis, the outer layer at a distance of 50.1 mm. The barrel covers

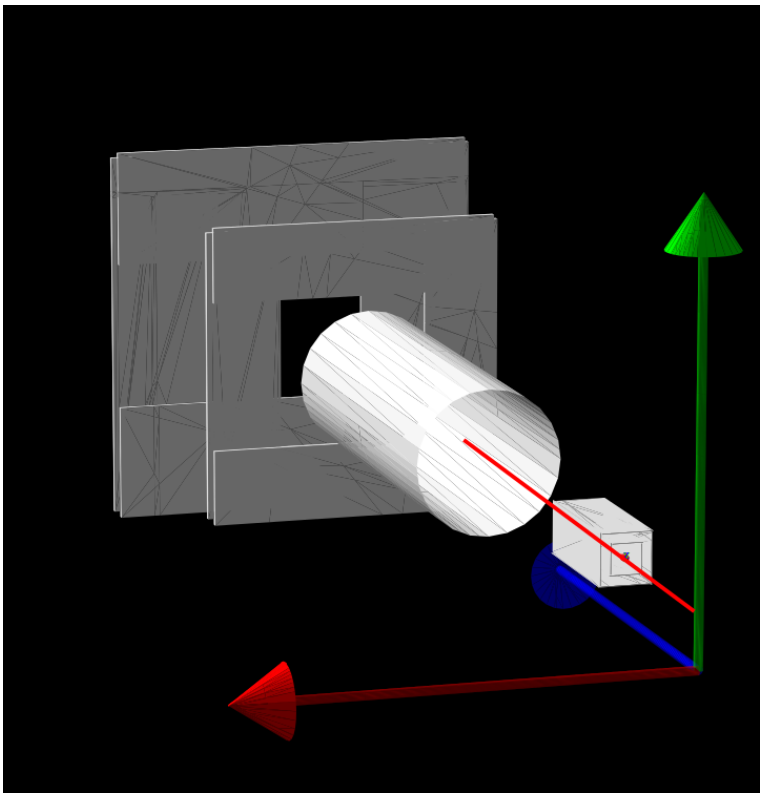

Figure 5: Schematic view of the simulated polarimeter used for beam reconstruction [11]. The diagonal red line indicates the beam direction. The cylinder at the center of the image is the beam tube. Only a part of it is shown to keep the view on the other detector parts free. The two square planes in the upper left corner are an endcap detector for forward scattered particles. It is not used in this analysis. The small cuboid in the lower right corner is the barrel section of the detector and consists of two layers of silicon strip detectors.

a θ range from 10° to 90°. The strip detectors in each layer are 100 μm thick. They are supported by a 1 mm thick layer of rohacell. The endcap is not used in this analysis.

When there is an elastic scattering event, the polarimeter can measure the hit positions of the two outgoing particles and the amount of energy they deposit in each detector layer. The hit positions correspond to a total of eight independent measured variables: two tracks times two detector layers times two coordinates to define a point on a plane. The energies are two more independent variables, but they are much less useful for beam reconstruction.

The simulation assumes that the experiment is performed using the cluster target at the COSY storage ring [12]. The lower density compared to a solid target reduces deflection of the beam particles which helps keeping the beam focused. Additionally it allows the outgoing particles to escape with negligible multiple scattering and energy loss. The target is simulated as a cuboid with the same particle density and rough physical dimensions as the cluster jet in the target. As the effects of the target on the track measurement are negligible compared to the detector uncertainty, the design of the target has no discernible effect on the beam reconstruction.

An earlier version of the beam phase space reconstruction algorithm was also tested with an experimental data set from a PhD thesis at the Forschungszentrum Jülich [14]. That data set was taken using a similar silicon detector with two detector planes on each side of the beam. The reaction was elastic scattering of protons with a kinetic energy of 44.8 MeV off a stationary deuteron target. This part of the analysis was given up as it became clear that the low energy led to very strong multiple scattering that increased the uncertainty of the incident particle direction to unacceptably high values. The resolution was in the order of 30 to 85 mrad and the plots showed strong stripe-like artifacts arising from the high strip widths.

3.4 Passage of Particles Through Matter

In the detector concepts used for this thesis, the outgoing particle tracks are measured with silicon detectors. Two effects are relevant for this measurement: multiple scattering and energy loss by interaction with electrons.

A charged particle moving through matter will lose energy to the electrons by exciting them to bound states with higher energy or to unbound states. The mean energy loss $\frac{dE}{dx}$ can be calculated using the Bethe-Bloch formula [15], which is valid over several orders of magnitude of the particle energy. The energy loss is plotted as a function of the particle's momentum in fig. 6. At the energies that appear in this thesis, $\frac{dE}{dx}$ decreases with increasing energy, i.e. particles with higher energy are less ionizing than

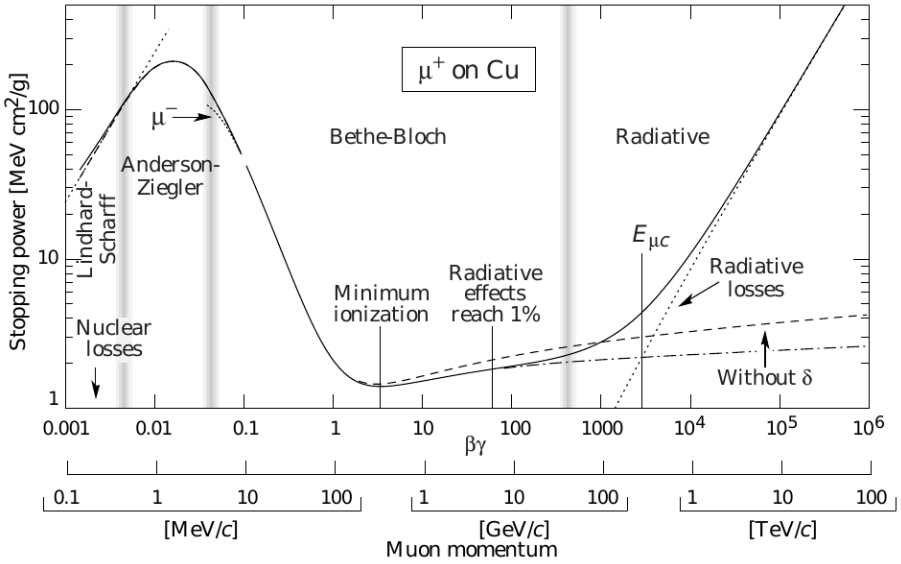

Figure 6: Mean energy loss of a heavy particle as a function of the kinetic energy [15, Review of Particle Physics, Chapter 27]. The plot is made for muons, but has the same form for all particles that are much heavier than electrons. The region relevant for this analysis is the declining region for energies below minimum ionization.

particles with lower energy. The energies are not so high that all particle speeds can be approximated as the speed of light. Therefore, particles of lower energy stay within the detector material longer than particles of higher energy. The energy loss scales with β^{-2}.

In thin layers like silicon detectors the energy loss fluctuates strongly. This is not a matter of the detector's energy resolution but a real physical effect. The probability distribution is typically asymmetric, with the higher tail falling more slowly than the lower tail. The mean energy loss described by the Bethe-Bloch formula is of limited use as a small percentage of particles that lose a high amount of energy contributes strongly to the mean, which leads to a high uncertainty. For particles with sufficiently high energy and layers that are not too thin, the distribution will approach a Landau distribution [15], whose expectation value diverges. The probability distribution does not typically have a closed-form representation. Even the aforementioned Landau distribution can only be expressed using integrals. The Landau theory and comparable approximations do not describe the particle energies and detector used in this thesis well.

It is also important to note that the energy loss is not exactly proportional to the length of the detector material traversed. The particle will lose more energy in a thicker detector than one would expect if the energy loss was proportional to the detector thickness.

For beam reconstruction the precise probability distribution of the deposited energy is required. Finding an adequate analytical expression is difficult, so a numerical approach based on the GEANT4 [13] package is used (section 4).

Heavy charged particles like protons and deuterons can also be deflected by multiple scattering with the nuclei in the detector material. This limits the accuracy of the track reconstruction because information on the particle's original direction is lost. Due to the central limit theorem, the probability density function for the scattering angles approaches a normal distribution near the mean value. The tails of the function will contain more events than in a Gaussian distribution. Like the deposited energy, the multiple scattering angle is simulated using GEANT4.

3.5 Principle of Reconstruction

Each elastic scattering event can be characterized by seven parameters:

- The center of mass scattering angle θ_{cm}
- The azimuth angle ϕ_{scat} describing the plane in which the outgoing tracks lie
- The position of the vertex in three dimensions $\mathbf{x}_{\mathrm{vertex}}$
- The parameters x' and y' to describe the direction of the incident particle

The vertex position and the direction of the incident particles are needed for beam phase space reconstruction, θ_{cm} and ϕ_{scat} are nuisance parameters describing the scattering process itself.

In order to reconstruct the position and direction of the incident particle, the tracks of both the ejectile and the recoil must be measured. The reconstruction of the position is based on the fact that the ejectile and the recoil come from the same vertex. Their tracks intersect within the uncertainty of measurement. Reconstructing θ_{cm} is not necessary to find the vertex, neither is any assumption about the kinematics or even the type of reaction.

Reconstructing the incident particle's momentum is more complicated. The tracks of the outgoing particles only define a plane in which the momentum vector must lie. Its direction within that plane depends on the scattering angles in the laboratory frame, which are a function of θ_{cm}. The scattering angles in the laboratory frame cannot be measured directly. In most experiments, the scattering angle in the laboratory frame is defined as the angle between the particle's track and the beam axis, implicitly assuming an ideal beam, which is a good approximation for many purposes. In this analysis, the deviation of the beam from the ideal behavior is the variable to be determined. The reconstruction of the incident particle's momentum reduces to the reconstruction of θ_{cm}.

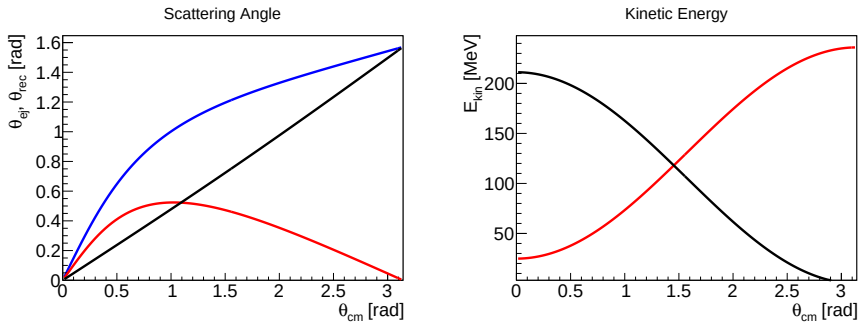

Figure 7: Left: Scattering angles for 236 MeV deuterons scattered off a proton target. The scattering angle of the outgoing deuteron (ejectile) is plotted in red, the angle of the proton (recoil) is plotted in black. The blue curve is the sum of the angles, the opening angle α. It can be measured without assuming the direction of the incoming beam. α is a bijective function of the center of mass scattering angle θ_{cm}. Right: Kinetic energies for the same reaction.

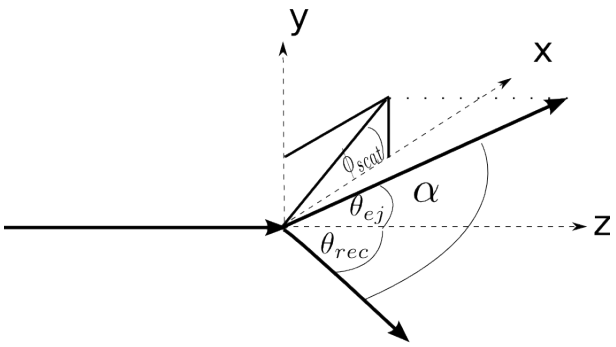

Figure 8: Definition of variables. For simplicity, the vertex is assumed to be at the origin of the coordinate system and the beam direction is assumed to be ideal.

What can be measured is the angle between the outgoing particles α, which is the sum of the scattering angles in the laboratory frame and therefore also a function of θ_{cm}. When α is known, θ_{cm} can be calculated by inverting the function. Another possibility is to measure the particles' energies, which are also functions of the scattering angle. Normally the measurement of hit positions is more precise than energy measurements, particularly energy measurement by means of the energy deposit in a thin slice. An exception might be scattering of identical particles at low energies. In the non-relativistic regime, the opening angle is always 90°. It only depends on θ_{cm} in the higher, relativistic terms. Fig. 7 shows α and the kinetic energies as a function of θ_{cm} for deuteron-proton scattering at 236 MeV. The precise reconstruction procedure is discussed in section 4.

4 Fitting Algorithm

4.1 Overview

The fitting procedure used to reconstruct the beam phase space is a kinematic maximum likelihood fit. For each elastic scattering event, the seven parameters introduced in section 3.5 are estimated based on the hit positions and deposited energies measured by the detector (section 3.3). The probability density function used for the fit is determined numerically using the detector response found in the Monte Carlo simulation.

As the errors for the different hits can be treated as statistically independent random variables, the likelihood function can be factorized into terms representing the inner hit positions, the outer hit positions and the deposited energies (section 4.3). As these likelihood functions are difficult to derive analytically they approximated by reference histograms filled with data from the Monte Carlo detector simulation (sections 4.5 and 4.6). The reference histograms are generated for discrete values of θ_{cm} covering the entire range of the detector acceptance.

The reconstruction then tries to find values for the event parameters for which the measured detector data appears likely. The fit estimates the likelihood of a measurement for a given set of parameter values by finding a reference histogram with similar θ_{cm} and checking how often the values for the measured variables appear there. As θ_{cm} will normally not be at a point where a reference histogram is available, the likelihood has to be calculated by interpolating between the neighboring points (section 4.4).

The actual minimizations is performed using the MIGRAD algorithm implemented in the MINUIT package [16, 17]. MIGRAD is a variable metric algorithm and calculates the function gradient to find minima, which means that it works best with continuously differentiable functions.

4.2 Maximum Likelihood Parameter Estimation

A maximum likelihood fit is a method to estimate the parameters of a probability density function. In this thesis, a maximum likelihood fit is used to find estimates for the the parameters described in section 3.5 based on the measured variables for each event.

A probability density function can be written as

$$f\left(\mathbf{x}|\mathbf{P}\right). \tag{4.1}$$

$\mathbf{x}$ represents a random vector, i.e. an ordered list of random variables and $\mathbf{P}$ represents all the parameters of the distribution. $\mathbf{P}$ is often called θ in statistical literature but was

renamed here to avoid confusion with the scattering angles. In the most general case, all entries in $\mathbf{x}$ are statistically dependent and each of them can depend on each parameter. A classical problem in statistics is to find an estimate for $\mathbf{P}$ given the functional form of f and a sample of a population of variables distributed according to f.

The maximum likelihood estimator $\hat{\mathbf{P}}$ [18] is defined as the set of parameters for which the probability density at $\mathbf{x}$ is maximal:

$$f\left(\mathbf{x}|\hat{\mathbf{P}}\right) = \max_{\mathbf{P}} f\left(\mathbf{x}|\mathbf{P}\right). \tag{4.2}$$

For beam phase space reconstruction $\mathbf{P}$ represents the set of seven parameters from section 3.5 that describe an elastic scattering event. $\mathbf{x}$ represents the detector measurements for one event. The next sections will deal with the numerical calculation of the probability density function that is used for the fit.

4.3 Numerical Calculation of Likelihood Function

To perform a maximum likelihood estimation, one has to know exactly how the distributions of the measured variables depend on the parameters. The polarimeter used in the simulation can measure the hit position and the deposited energy in each layer for both the ejectile and the recoil track. The random vector is $\mathbf{x} = \{\mathbf{x}_{\mathrm{ej},1},\ \mathbf{x}_{\mathrm{ej},2},\ \mathbf{x}_{\mathrm{rec},1},\ \mathbf{x}_{\mathrm{rec},2},\ \Delta E_{\mathrm{ej},1},\ \Delta E_{\mathrm{ej},2},\ \Delta E_{\mathrm{rec},1},\ \Delta E_{\mathrm{rec},2}\}$. The index 1 denotes the values measured in the inner detector layer, the index 2 denotes those measured in the outer layer. The indices "ej" and "rec" stand for ejectile and recoil. $\mathbf{x}_{\mathrm{ej,rec},1,2}$ is the hit position, ΔE is the deposited energy.

The form of the likelihood function can be simplified by assuming that the variables are statistically independent, which means their multivariate probability distribution can be factorized into parts that only depend on one variable each. This assumption is justified by the fact that they are the results of independent measurement. This yields the form

$$\begin{aligned} f\left(\mathbf{x}|\mathbf{P}\right) = {} & f\left(\mathbf{x}_{\mathrm{ej},1}|\mathbf{P}\right) \cdot f\left(\mathbf{x}_{\mathrm{ej},2}|\mathbf{P}\right) \\ & \cdot f\left(\mathbf{x}_{\mathrm{rec},1}|\mathbf{P}\right) \cdot f\left(\mathbf{x}_{\mathrm{rec},2}|\mathbf{P}\right) \\ & \cdot f\left(\Delta E_{\mathrm{ej},1}, \Delta E_{\mathrm{ej},2}|\mathbf{P}\right) \cdot f\left(\Delta E_{\mathrm{rec},1}, \Delta E_{\mathrm{rec},2}|\mathbf{P}\right) \end{aligned}. \tag{4.3}$$

The energies measured in the inner and outer layers were not factorized because they cannot be treated as independent. This is because the amount of energy a particle loses in the two layers is correlated over the thickness of detector material passed and

because the energy loss in the first layer determines a particle's kinetic energy when it hits the second layer. For numerical calculations, the logarithm of the likelihood is more manageable than the likelihood itself. The maxima are less sharp and extremely small likelihoods do not reach the limits of numerical precision as quickly as without the logarithm.

$$\begin{aligned}\log\left(f\left(\mathbf{x}|\mathbf{P}\right)\right) = &\log\left(f\left(\mathbf{x}_{\mathrm{ej},1}|\mathbf{P}\right)\right) + \log\left(f\left(\mathbf{x}_{\mathrm{ej},2}|\mathbf{P}\right)\right) \\ &+ \log\left(f\left(\mathbf{x}_{\mathrm{rec},1}|\mathbf{P}\right)\right) + \log\left(f\left(\mathbf{x}_{\mathrm{rec},2}|\mathbf{P}\right)\right) \\ &+ \log\left(f\left(\Delta E_{\mathrm{ej},1}, \Delta E_{\mathrm{ej},2}|\mathbf{P}\right)\right) + \log\left(f\left(\Delta E_{\mathrm{rec},1}, \Delta E_{\mathrm{rec},2}|\mathbf{P}\right)\right)\end{aligned} \quad . \tag{4.4}$$

In order to perform the fit, one needs an estimate for each of the summands in (4.4). It is very difficult to find analytical expressions because the distributions depend on specifics of the detector design and because some of them are obtained by solving transport equations that are quite complicated even for simple geometries. To avoid that problem, a numerical approach based on a GEANT4 simulation of the detector [11] is used. The relevant processes are almost completely electromagnetic and can be simulated to a high accuracy.

The basic idea is to generate a series of reference histograms for known event parameters $\mathbf{P}$. These histograms can be used as an approximation for the distribution of their respective variables and are used as a lookup table. When the fit routine later calculates the likelihood of the measured variables for some parameters, it finds reference histograms with similar parameters and looks how often the measured values appear there. This provides a estimate for the likelihood.

When generating the reference histograms, the beam is assumed to be ideal: $x' = y' = 0$ and $\mathbf{x}_{\mathrm{vertex}} = \mathbf{0}$. The azimuth angle ϕ_{scat} is distributed uniformly. These parameters can all be reduced to translations or rotations of the beam and the outgoing tracks. Their influence on the probability density functions can therefore be calculated semianalytically using geometrical calculations and a reference point for some fixed value. The parameter θ_{cm} is set to a series of different discrete values that cover the entire range of events that lie within the acceptance of the detector. A number of events is generated at each value of θ_{cm}. At the end, one has histograms for the various measured variables for every value of θ_{cm}.

In section 4.5 and 4.6 it will be shown that all required distributions can be obtained from histograms of the angle θ_{ms} by which multiple scattering deflects the particles in the first detector layer and two-dimensional histograms of the energies ΔE_1 and ΔE_2

deposited in the inner and outer layers of the detector divided by the width of detector material traversed d. In conclusion, the procedure to find the distributions is:

1. Pick discrete values of θ_{cm} covering the entire variable range.
2. At each value, generate a number of Monte Carlo events. Assume a uniform distribution of ϕ_{scat} and a perfect beam.
3. At each value, fill histograms of θ_{ms} for the ejectile and the recoil. Fill 2D histograms for $\frac{\Delta E_1}{d}$ and $\frac{\Delta E_2}{d}$ for the ejectile and the recoil.
4. Use these histograms to estimate the likelihood in the fit.

4.4 Interpolation

The minimization algorithm used in the fit must be able to calculate the likelihood for all possible values for the measured variables and the parameters. The reference histograms are only available for discrete values of θ_{cm} and the histograms themselves have discrete bins. It is therefore necessary to interpolate between the points. The interpolation should be continuously differentiable so that a minimization algorithm that follows a gradient will not run into discontinuities. This can be achieved using the Akima interpolation algorithm [19]. It resembles a cubic spline interpolation as it uses third degree polynomials to interpolate between the points. The difference to spline interpolation is that the derivatives at the given points are estimated locally from the neighboring points rather than by solving a linear system of equations. This makes the interpolation computationally faster and assures that a single reference point can only influence the interpolation function locally and not globally.

In addition to the one-dimensional interpolation used for θ_{cm}, the fit uses two-dimensional interpolation to determine the likelihood of the deposited energy from the values at the discrete bin centers of the reference histograms. This is a trivial generalization of the one-dimensional Akima interpolation and can be constructed in analogy to a two-dimensional spline interpolation in [20, section 3.6.2]. Given the function values on a regular lattice (x_i, y_j) and a point (x_0, y_0) at which the function has to be evaluated, one can first perform a one-dimensional interpolation along x for each y_j to estimate the function values at (x_0, y_j). The remaining problem is another one-dimensional interpolation in y_i.

4.5 Hit Positions

The particle hit positions are the most important variables for the beam reconstruction as they provide much more precise information than the deposited energies. There are two

reasons for uncertainties in the measurement of hit positions: the geometrical resolution of the detector and multiple scattering. The error from the strip pitch is simulated by rounding the exact results given by the simulation to the nearest integer multiple of an assumed strip pitch. This is equivalent to using the center of the strip that was hit by a particle as an estimator for the true hit position. Multiple scattering is handled by the GEANT4 simulation.

In silicon strip detectors, the resolution is limited by the width of the strips or by the width of a number of strips connected to the same readout channel. Particles coming from the target can be deflected as they move trough the inner detector layer, which limits the accuracy to which the track direction can be reconstructed. For the outer detector layer one has to consider multiple scattering as well. For a strip pitch in the order of $100\,\mu$m, this is the dominant error. As the inner and outer detector hits are affected by different errors, they are modeled differently for the probability density function.

For the inner detector layer the only significant error is the binning error from the finite size of the strips. This error is not truly random, it results from a deterministic rounding operation. If the event parameters are known, the tracks are fixed and can be calculated. Only one strip in the detector could possibly be hit, there is only one discrete possible outcome for the measurement. Binning and digitization errors are can be modeled as uniform distributions. If that model is used the likelihood is constant for all points in parameter space for which the tracks hit the same strip as in the measurement, the likelihood is zero for all other parameters.

From a numerical point of view the uniform distribution is difficult to handle. It is discontinuous and its derivative is zero for all points except the discontinuities, at which it is undefined. Apart from that, the logarithm of a likelihood of zero is undefined. For those reasons, the probability density function for the inner hits is approximated by a normal distribution with a standard deviation equal to the strip pitch divided by the square root of twelve, the same standard deviation as for a uniform distribution over the strip width. The maximum of the distribution is at the strip's center.

The error of the outer hit position measurement comes from the detector resolution and multiple scattering in the inner detector layer. There are two independent outer hit coordinates for each track, so in general the probability density must be bivariate. Using symmetry, it is possible to simplify it to a distribution of only one variable. It is useful to define the multiple scattering angle θ_{ms}

$$\cos\left(\theta_{\mathrm{ms}}\right) = \frac{\left(\mathbf{x}_2 - \mathbf{x}_1\right) \cdot \hat{\mathbf{p}}\left(\mathbf{P}\right)}{\left|\mathbf{x}_2 - \mathbf{x}_1\right|}, \tag{4.5}$$

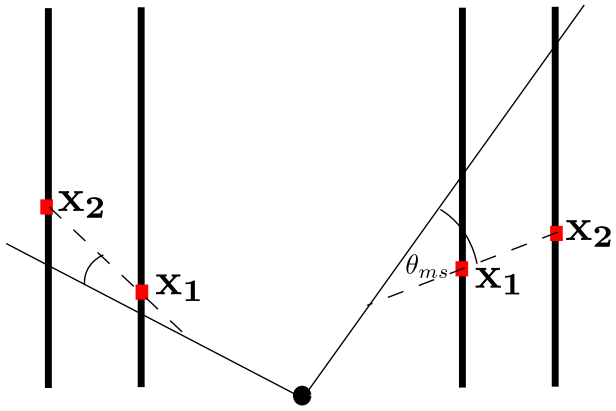

Figure 9: Illustration of the definition of θ_{ms}. The red squares are the measured detector hits, the thick lines are the silicon detectors, the thin solid lines are the tracks calculated from the event parameters.

where $\hat{\mathbf{p}}$ is the unit vector pointing in the direction of the particle's momentum calculated from the event parameters. $\mathbf{x}_1$ and $\mathbf{x}_2$ are the measured hit positions in the inner and outer detector layer. The index in θ_{ms} stands for multiple scattering, but it is defined as the angle between the measured track and the theoretical one regardless of the cause of the deviation. The errors of $\mathbf{x}_1$ and $\mathbf{x}_2$ that are due to the detector resolution are also included. The likelihood for the outer hit position is equivalent to the likelihood of θ_{ms} because multiple scattering is a radially symmetric process, which means that only the total angle but not the direction of multiple scattering contribute the the likelihood function.

The distribution of θ_{ms} used for the fit is extracted from the reference histograms (section 4.3). In principle it depends on the particle's momentum, which is a function of θ_{cm} and on the slant thickness of the detector material traversed, which is a function of all parameters except the vertex position. To simplify the calculation, only the dependence on θ_{cm} is taken into account. x' and y' are neglected, ϕ_{scat} is averaged over all possible values. The angle distribution for multiple scattering approaches a Gaussian distribution around the mean value, the tails contain more events than those of a Gaussian distribution [15, chapter 27]. The limited resolution for $\mathbf{x}_1$ and $\mathbf{x}_2$ will smear out the distribution, but not change its basic shape.

The distribution of $\mathbf{x}_2$ can be modeled more precisely by the formula

$$f\left(\mathbf{x}_2\right) = A \cdot \left(1 + B \cdot \frac{\theta_{\text{ms}}^{\epsilon}\left(\mathbf{x}_2\right)}{\nu}\right)^{-\frac{\nu+1}{2}}. \tag{4.6}$$

This distribution resembles a t-distribution, except that the exponent ϵ is a free parameter and not fixed to 2. The distribution becomes Gaussian for $\nu \to \infty$ and $\epsilon = 2$. A is a normation constant, B is a parameter for the width. In the Gaussian limit B is the inverse variance. For small ν, the tails become heavier, for large ν they become more Gaussian. The exponent ϵ models the shape of the distribution around the center. The parameters in (4.6) are extracted from fits to the reference histograms of θ_{ms}. Note that the distribution of θ_{ms} is actually

$$f\left(\theta_{\mathrm{ms}}\right) = \theta_{\mathrm{ms}} \cdot A \cdot \left(1 + B \cdot \frac{\theta_{\mathrm{ms}}^{\epsilon}}{\nu}\right)^{-\frac{\nu+1}{2}} . \tag{4.7}$$

The additional factor θ_{ms} is a Jacobian determinant. This becomes evident when considering the fact that θ_{ms} was introduced to simplify a bivariate distribution. (4.6) is the probability per interval of $\mathbf{x}_2$, which has to be maximized, while (4.7) is the probability per interval of θ_{cm}, which is plotted in the reference histogram. Thus (4.6) is used when evaluating the likelihood in the fit, (4.7) is used to determine the parameters from the reference histograms.

Figs. 10 and 11 show the distribution of θ_{ms} for various values of θ_{cm}. The fit function is an adequate approximation for all histograms.

4.6 Deposited Energy

The deposited energy in each detector hit can provide additional information on an elastic scattering event. It is much less precise than the measurement of the hit positions but can be used as a supplement to improve precision. When a charged particle passes a thin layer of material like a silicon detector, it will lose some energy due to interaction with electrons in the material. The amount of energy fluctuates statistically; the probability distribution is often heavy-tailed and does not have a simple analytical representation (see also section 3.4).

The deposited energies in the first and second layer (ΔE_1, ΔE_2) are not statistically independent. The probability density function cannot be factorized:

$$f\left(\Delta E_1, \Delta E_2\right) \neq f\left(\Delta E_1\right) \cdot f\left(\Delta E_2\right) .$$

The energies are correlated over the effective thickness of detector material traversed, which will be shown later in this section. Apart from that, particles may lose a significant fraction of their energy in the first layer, which slows them down. As the particle energies lie in the range where $\Delta E \propto \beta^{-2}$, slower particles become more strongly ionizing. That

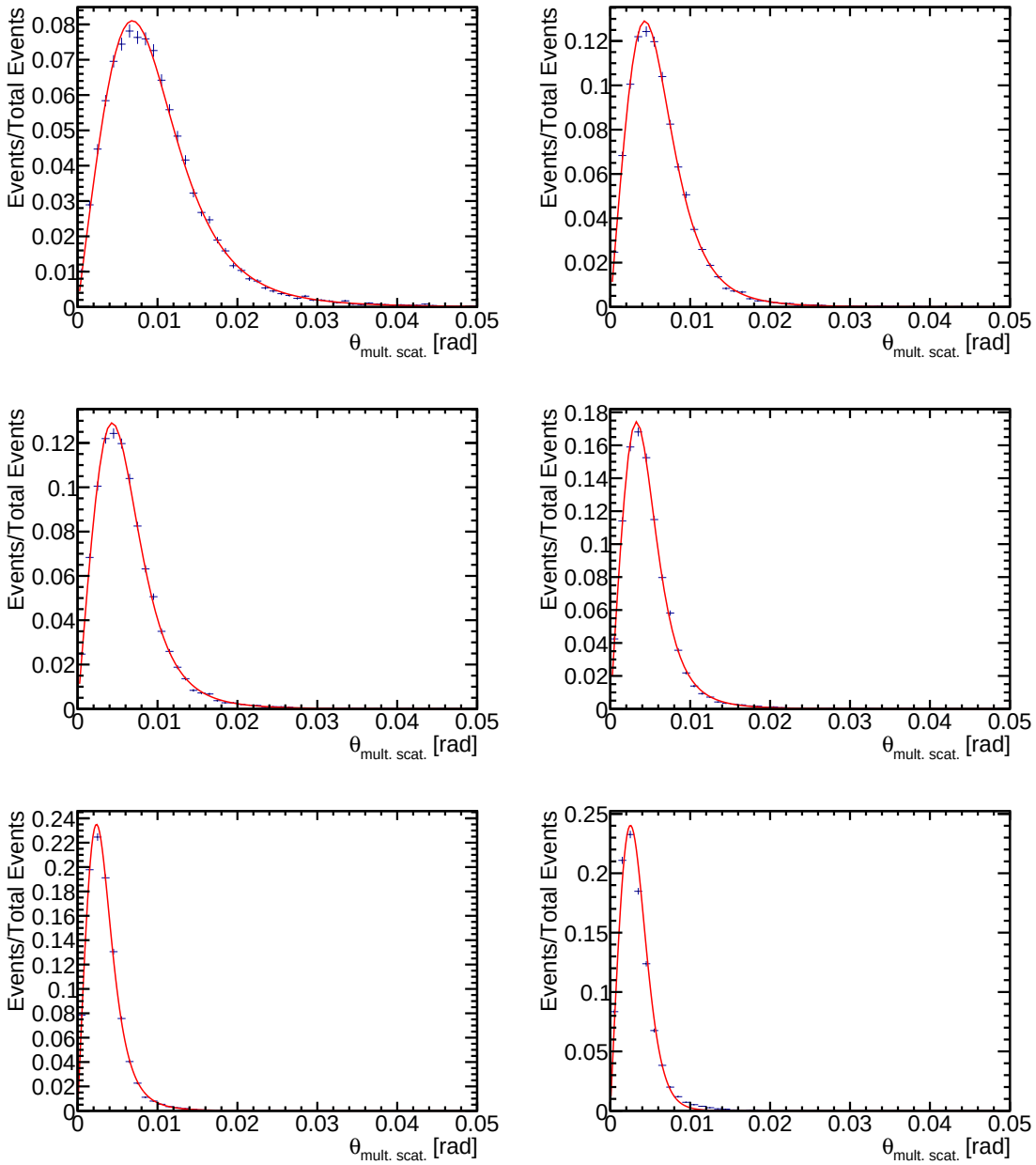

Figure 10: Ejectile multiple scattering angle $\theta_{\rm ms}$ plotted for $\theta_{\rm cm} = 0.71$, 1.01, 1.31, 1.61, 1.91, 2.21 (left to right, top to bottom). The histograms are normalized so that the sum of all bins is 1. The red curves are fits of the distribution (4.7).

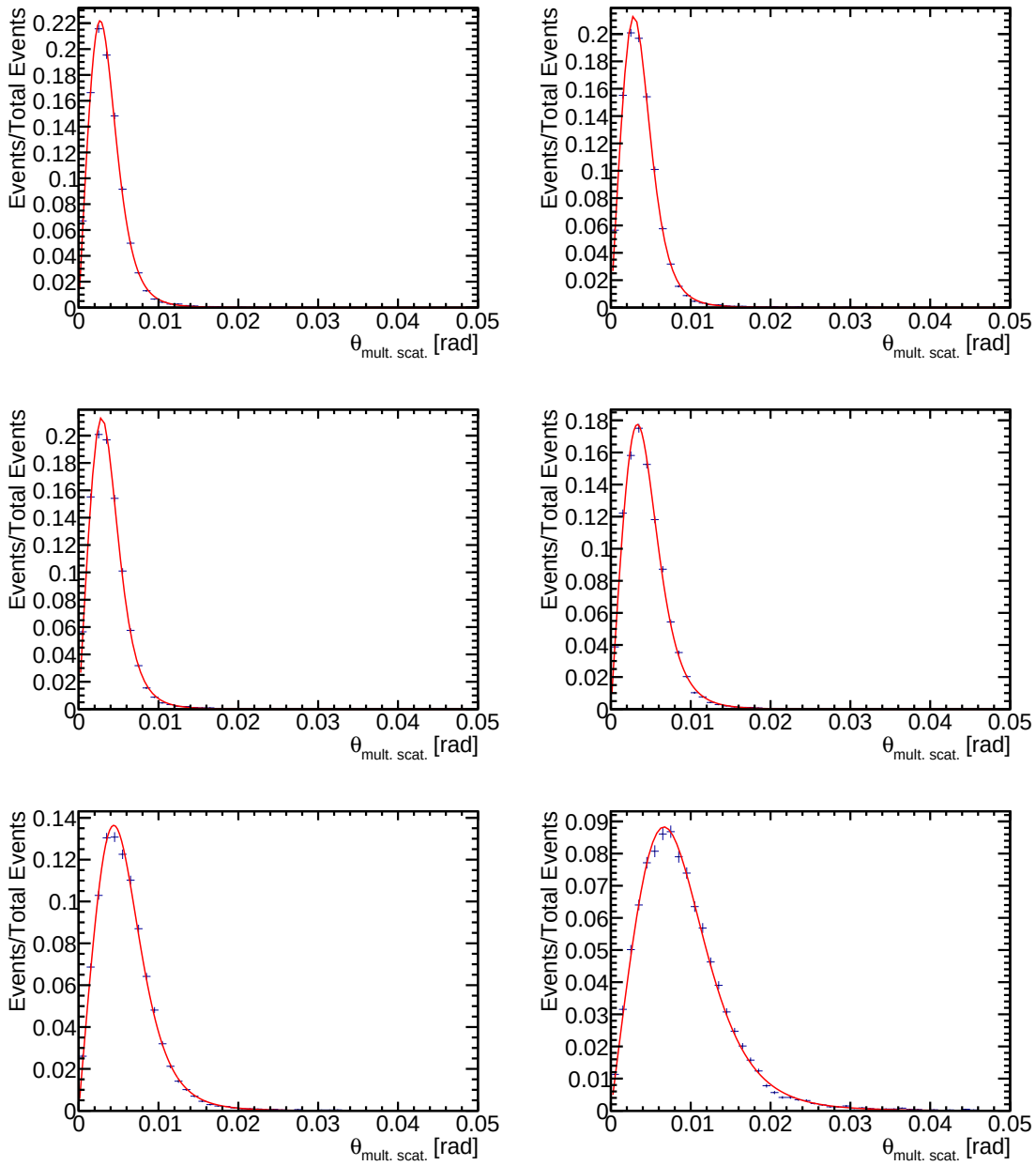

Figure 11: The same as fig. 10 for the recoil.

means that a particle that has lost a large amount of energy in the first layer because of a statistical fluctuation is likely to lose a higher than average amount of energy in the second layer. This effect is especially strong for particles with low energies. For the detector used here it does not play an important role, the typical energy loss is in the order of 200 keV while kinetic energies are in the order of 100 MeV. It would become more important for scattering at lower energies.

The amount of energy a particle loses when passing a detector layer depends on its charge, its kinetic energy and on the thickness of the detector material. The charge is always +1 e for protons and deuterons and does not influence the probability distribution. The kinetic energy can be calculated from the center of mass scattering angle θ_{cm} alone. The thickness of the detector layer is a known parameter of the experimental setup. It has to be corrected for the angle of the particle because a particle hitting the detector at a flat angle δ effectively passes more material.

$$d = \frac{d_0}{\cos\delta} \tag{4.8}$$

d is the effective thickness of the material, d_0 is the thickness measured the normal way, perpendicularly to the surface. δ is the angle between the particle track and the normal vector to the detector surface. d is a function of θ_{cm}, ϕ_{scat}, x' and y'. The vertex position does not influence the angle between the tracks and the detector for planar detectors as they are used in this simulation. It does influence which side of detector is hit though, thus having an indirect influence on the angle.

To leading order, the deposited energy ΔE is proportional to d. Hence $\frac{\Delta E}{d}$ depends only weakly on the detector thickness and mostly on the particle's kinetic energy $E_{\mathrm{kin}}(\theta_{\mathrm{cm}})$. Using a simple transformation of variables, the likelihood for the deposited energies can be written as

$$\begin{aligned} f(\Delta E_1, \Delta E_2|\mathbf{P}) &= f\left(\frac{\Delta E_1}{d_1(\mathbf{P})}, \frac{\Delta E_2}{d_2(\mathbf{P})}\middle|\theta_{\mathrm{cm}}\right) \cdot \frac{1}{d_1(\mathbf{P})\, d_2(\mathbf{P})} \\ &= f\left(\frac{\Delta E_1}{d(\mathbf{P})}, \frac{\Delta E_2}{d(\mathbf{P})}\middle|\theta_{\mathrm{cm}}\right) \cdot \frac{1}{d(\mathbf{P})^2}. \end{aligned} \tag{4.9}$$

d was assumed to be equal for both detector layers. For the detector used here this is a very good approximation as the planes are parallel and the particle direction changes only slightly due to multiple scattering. For different detectors d_1 and d_2 might differ. The approximation $\Delta E \propto d$ works best for particles with high energies, but is adequate over most of the range of energies that appear in the elastic scattering reaction studied

here. Fig. 12 shows the dependence of $\Delta E_2/d$ on d for the greatest and the smallest values of θ_{cm} used, corresponding to the greatest and smallest kinetic energies. $\Delta E_2/d$ changes by $\sim 25\%$ in the worst cases and is constant within the statistical errors in the best.

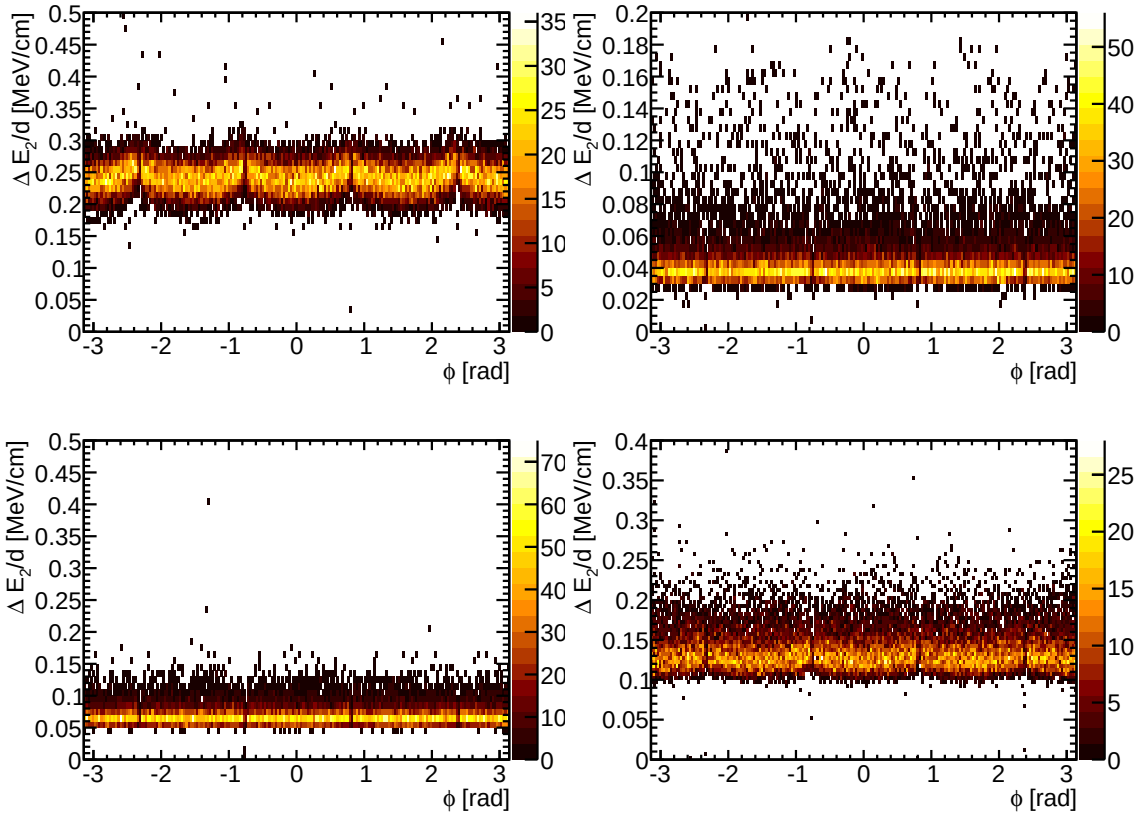

Figure 12: Dependence of $\Delta E_2/d$ on ϕ_{scat} for $\theta_{\mathrm{cm}} = 0.71$ (top, highest recoil kinetic energy, lowest ejectile kinetic energy) and $\theta_{\mathrm{cm}} = 2.21$ (bottom, highest ejectile kinetic energy, lowest recoil kinetic energy). The left plots show the histograms for the ejectile tracks, the right plots for the recoil tracks. d varies by a factor of $\sqrt{2}$ between tracks that hit the center of a detector plane ($\phi_{\mathrm{scat}} \in \{-\pi/2,\ 0,\ \pi/2,\ 3\pi/2\}$) and tracks that hit a corner (off by $\pi/4$).

The variable transformation in (4.9) has several advantages: it eliminates a significant part of the correlation between the two variables, it leads to a sharper overall distribution and it simplifies the way the likelihood depends on the event parameters. The left side of (4.9) is the likelihood needed for the fit. The expression on the left hand side divides it into

the distribution $f\left(\frac{\Delta E_1}{d(\mathbf{P})}, \frac{\Delta E_2}{d(\mathbf{P})}\middle|\, \theta_{\mathrm{cm}}\right)$, which for which the dependence on all parameters except θ_{cm} is neglected, and the factor $\frac{1}{d(\mathbf{P})^2}$, which can be calculated analytically from the event parameters. The distribution of $\frac{\Delta E}{d(\mathbf{P})}$ can be extracted from the reference histograms.

Examples of distributions can be seen in figs. 13 and 14. The width of the distributions is large compared to the how much the mean value moves for different values of θ_{cm} which limits the usefulness of ΔE for reconstruction.

When the fit routine calculates the likelihood, it first calculates $\frac{\Delta E}{d(\mathbf{P})}$ and then looks up the likelihood of the value in the reference histogram. Finally the result is divided by d^2. For some combinations of parameters and measured energies it is not possible to look up a meaningful likelihood in the histograms, most importantly when the respective bin is empty. Returning zero is not an option because the fitting routine maximizes the logarithm of the likelihood, which would tend to $-\infty$.

Even for bins that contain a small but nonzero number of events, the associated likelihood will be mostly meaningless. The bins in the tails of the distributions have errors to their contents that are in the same order of magnitude as the bin content itself. For those bins the variation from one bin to the next will be dominated by noise rather than the difference in the true likelihoods. The fitting procedure neglects all Monte Carlo errors and will treat them as real. The problem could be mitigated by generating more events for the reference histograms, but there would always be some bins that are noise dominated. Fig. 15 shows a logarithmic plot of one of the reference histograms, in which the noise becomes more visible. The bin content becomes less smooth for bins in the tails.

To prevent noise dominated bins from influencing the final fit, a threshold parameter is introduced. All bins whose content is greater than the threshold are assumed to represent meaningful likelihoods. Bins below the threshold are assumed to be noise only. The fit routine sets the content of those bins equal to the threshold. This means that the likelihood is assumed to be constant for values of $\frac{\Delta E}{d(\mathbf{P})}$ that lie outside the reference histogram. The likelihood at the bin centers is

$$f\left(\frac{\Delta E_1}{d\,(\mathbf{P})}, \frac{\Delta E_2}{d\,(\mathbf{P})}\middle|\, \theta_{\mathrm{cm}}\right) = \begin{cases} \frac{N_{\text{Events, bin}}}{N_{\text{Events, total}}} & \frac{N_{\text{Events, bin}}}{N_{\text{Events, total}}} > \text{Threshold} \\ \text{Threshold} & \frac{N_{\text{Events, bin}}}{N_{\text{Events, total}}} < \text{Threshold} \end{cases}. \tag{4.10}$$

The likelihood at all other points is determined using two-dimensional interpolation.

The fit will not usually converge on these points because such outliers in energy are extremely unlikely. Yet it is necessary to be able to compute a meaningful likelihood

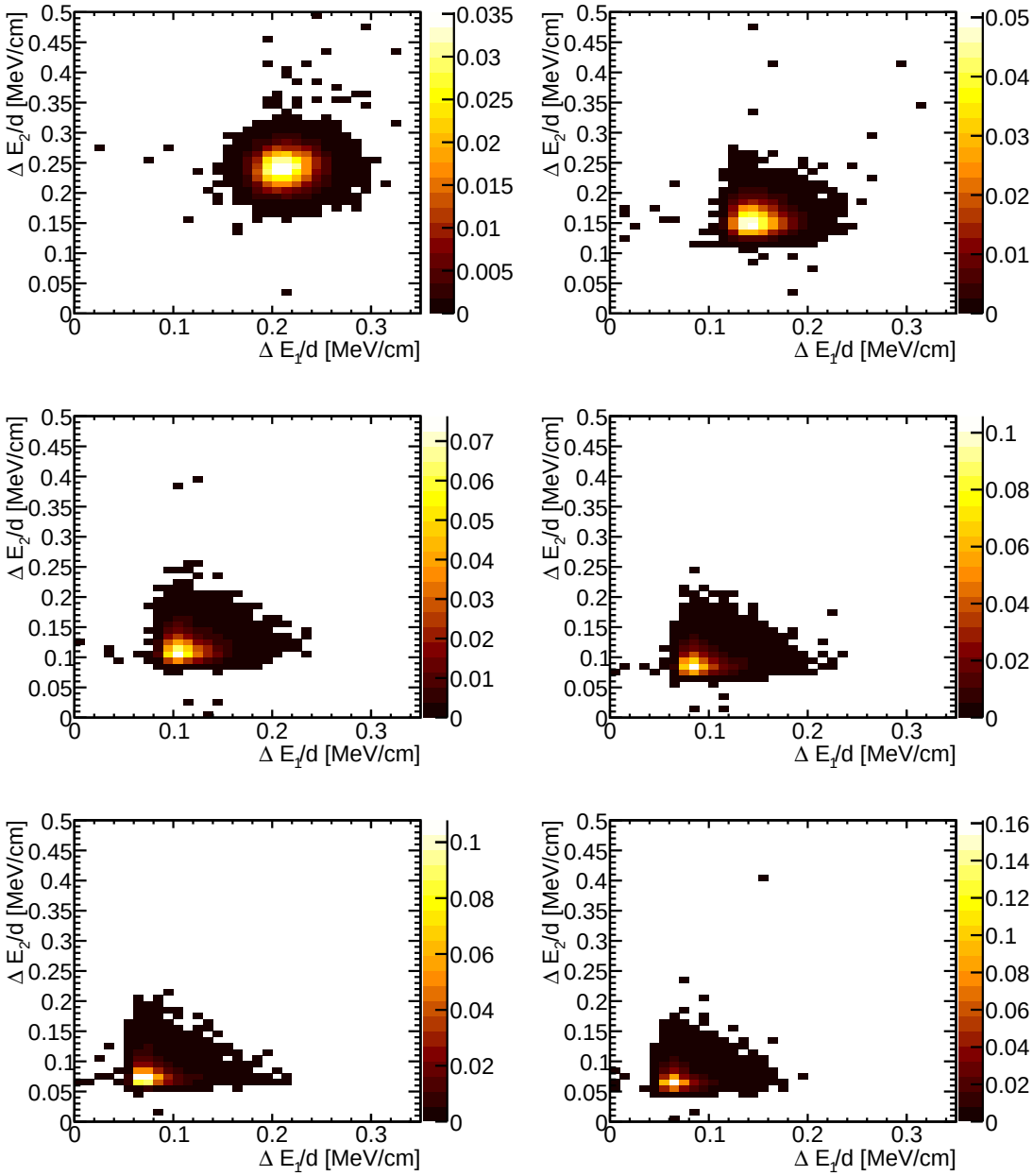

Figure 13: $\frac{\Delta E_1}{d}$ and $\frac{\Delta E_2}{d}$ plotted for the ejectile for $\theta_{\mathrm{cm}} = 0.71$, 1.01, 1.31, 1.61, 1.91, 2.21 (left to right, top to bottom). The histograms are normalized so that the sum of all bin contents is 1. The deposited energy decreases with increasing θ_{cm} as the ejectile's energy increases. The distributions are broad and do not change strongly with θ_{cm}, yet there is some sensitivity.

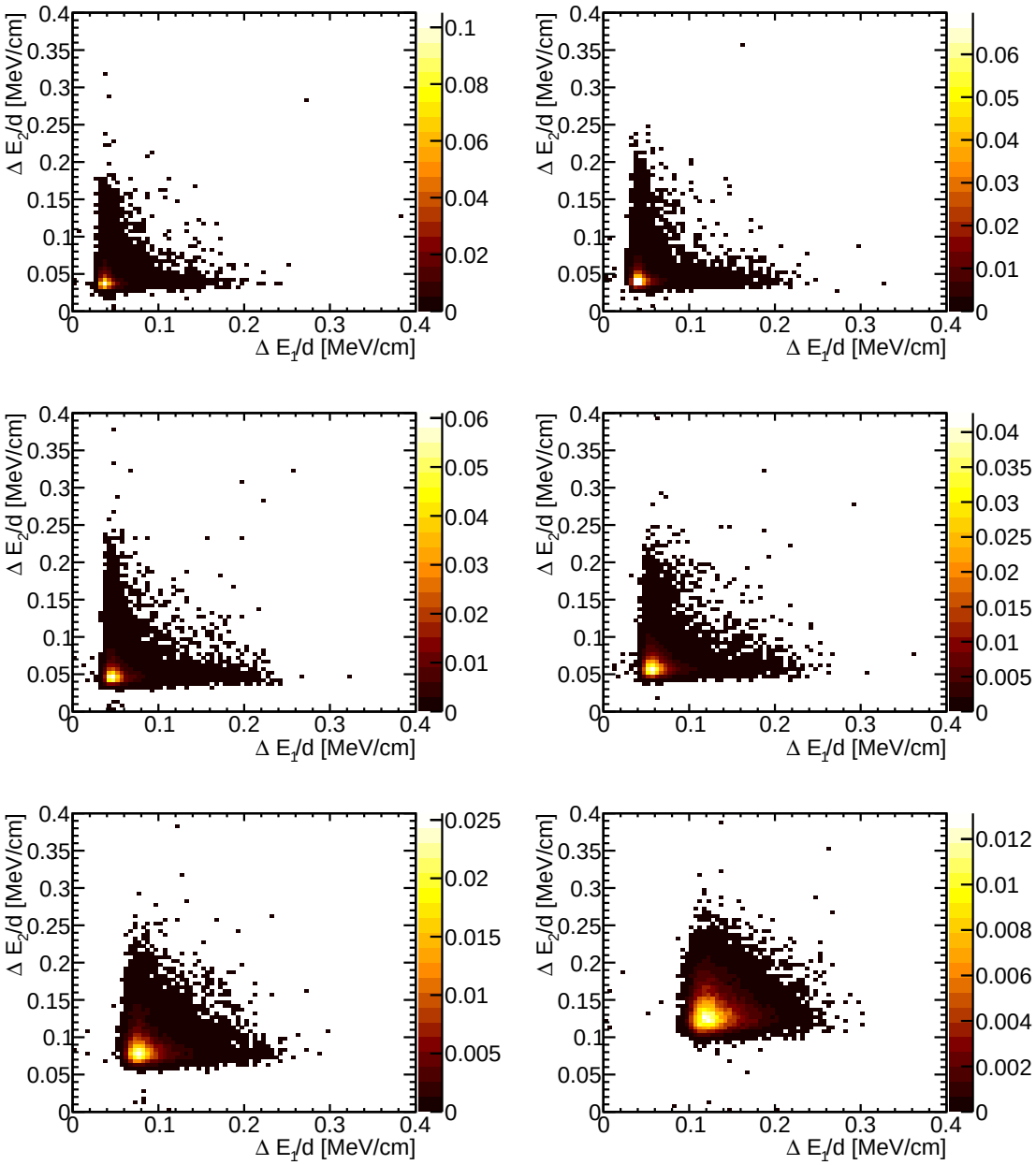

Figure 14: Same as fig. 13 for the recoil. Here the deposited energy increases with increasing θ_{cm} as the recoil's kinetic energy decreases.

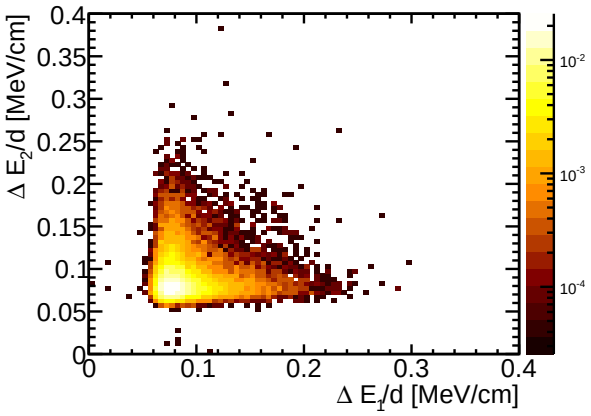

Figure 15: Logarithmic plot of the reference histogram for the recoil energy at $\theta_{cm} = 1.91$. The bins in the tail of the distribution are dominated by noise.

even for these cases, because the fitter might set the parameters to values that lie far from the true ones in intermediate steps. For instance, if the true θ_{cm} is around 1.6, $\frac{\Delta E}{d(\mathbf{P})}$ might be around 0.06 MeV/cm for the recoil in both layers. The fitter might yet compute the likelihood for $\theta_{\mathrm{cm}} = 1.9$ and find the bins in the corresponding reference histogram empty, which makes it necessary to make an assumption for the likelihood. The bins that are changed by (4.10) are far from the global maximum of the likelihood and will not influence it significantly.

5 Results

5.1 Settings

The beam phase space reconstruction is tested with Monte Carlo Data. The difference between the known true event parameters and the results from the fit can be used to estimate the statistical and some systematic errors in the procedure. The fit performance is tested at several fixed benchmark points in the beam phase space in order to study how the distribution of errors depends on the beam.

The fit accepts events with exactly two detector hits. The opening angle of the tracks must be between 0.82 and 1.4 rad to avoid events in which either particle has a very low energy. One million primary events are generated for the test sample, corresponding to around 350000 events meeting the criteria.

The reference histograms are generated for 175 discrete values of θ_{cm} distributed evenly between 0.69 and 2.37 rad. 25000 events are generated at each point. Unless otherwise specified, the strip pitch is 100 μm and the noise suppression threshold for the deposited energy in (4.10) is 10^{-3}.

5.2 Distribution of Errors

Fig. 16 shows the distributions of x', y', x and y for an ideal beam reconstructed using only the hit positions and reconstructed using hit positions and deposited energies. All distributions have sharp peaks at the center and a relatively large number of outliers. This is not surprising as the distribution of the multiple scattering angle, which is the main source of errors, is a similarly heavy-tailed distribution. A handful of events are reconstructed at even larger angles, up to 0.5 rad. Although these events make up only a tiny percentage of the total number, they can distort the sample average and standard deviation. The plots for the ideal beam show that using the deposited energy leads to a decrease in the statistical errors for x' and y' while having no strong influence on x and y.

There is a strong negative correlation between x and x', and between y and y', which is shown in fig. 17. This is not a real feature of the data but an effect of the fit. The errors of fit parameters are typically correlated unless a parametrization is constructed specifically to avoid this. If the fitting algorithm overestimates x, it is likely to underestimate x'. The same correlation is found for y and y'. This effect is interesting as plots of the beam position and angle could be used in calibration to find the point at which the beam is focused to its smallest diameter. If one measured a distribution of x' and x in which the variables were truly negatively correlated, not just by an effect of the measuring errors,

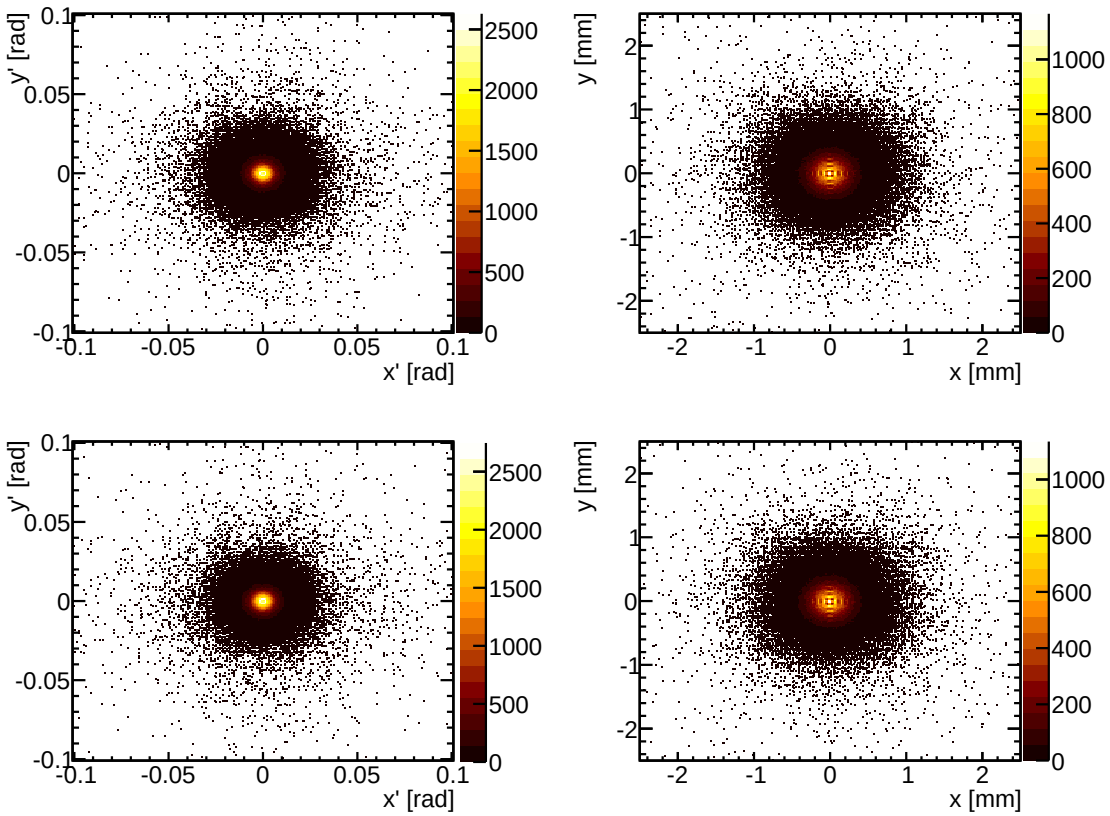

Figure 16: Beam angle and position reconstructed for an ideal beam. Top: distributions of x', y', x and y reconstructed using only the hit positions. Bottom: the same fit using the deposited energy as well. All distributions contain a large number of outliers. The distribution of x and y shows artifacts from the discrete readout of the silicon strip detector.

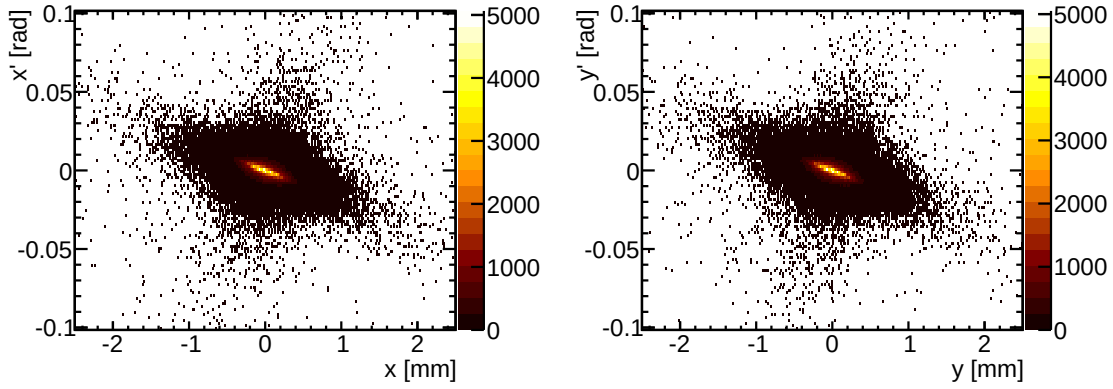

Figure 17: Correlation between reconstructed beam position and angle for an ideal beam. There is a strong correlation between x and x', and between y and y'.

that would mean that the distribution of x would become narrower downstream from the detector. Conversely, a distribution in which x' and x are truly positively correlated would mean that the width of the distribution of x would decrease downstream from the detector and that the focal point is upstream. The correlation from the fit means that this is unlikely to work in practice.

For non-ideal beams, the distributions change in shape. The outliers are much more widely and irregularly distributed. Fig. 18 shows the fit result distributions for some non-ideal beam configurations. While the peak of the distribution is still at the true position, the outliers reach a lot farther than for the ideal beam. It is easy to see that a sample mean value is not a good estimator for the true beam parameters.

To suppress the influence of outliers, the sample mean and standard deviation will be calculated considering only those bins whose content is no smaller than 1% of the maximum bin content in a given histogram. In principle the mode of the distribution would be a better estimator, but it is hard to determine due to the stripe artifacts introduced by the discrete silicon strip detector readout, especially in the distributions for x and y.

The statistical errors of x', y', x and y depend on the true beam parameters. Fig. 19 shows the width of the distribution as a function of x' for an otherwise ideal beam. Fig. 20 shows similar plots as a function of the true x. Each point is the sample standard deviation of one million test events. The beam was simulated as ideal except for the parameter on the abscissa, x or x'. Due to symmetry the plots of y and y' would look almost the same. y and y' do not depend significantly on x and x'. Typical misalignments

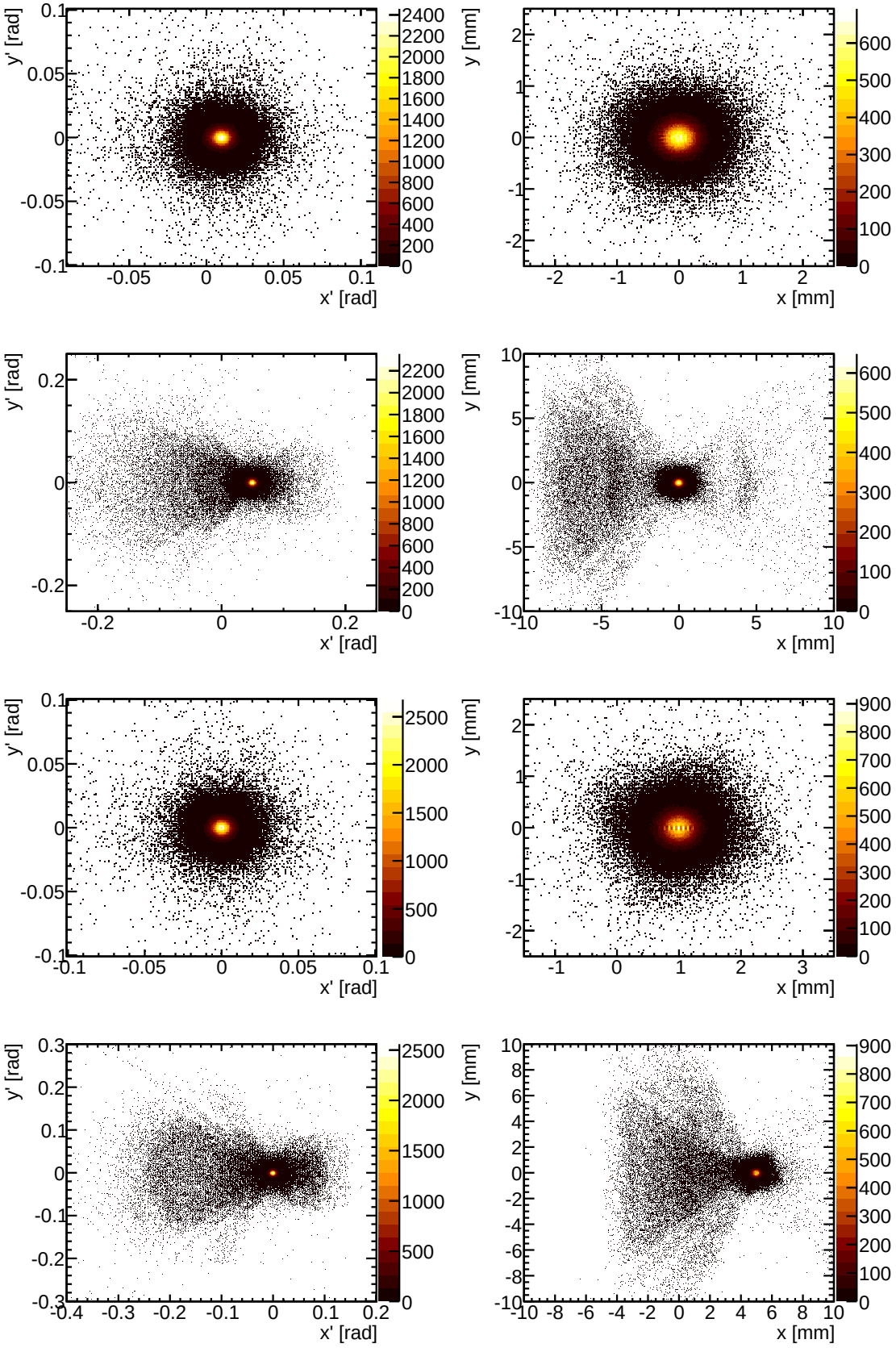

Figure 18: Reconstructed beam angle and position distributions for $x' = 10\,\text{mrad}$ (first row), $x' = 50\,\text{mrad}$ (second row), $x = 1\,\text{mm}$ (third row) and $x = 10\,\text{mm}$ (last row). The more the beam deviates from the ideal position and direction, the wider the distribution of outliers becomes. The peak is still at the true value.

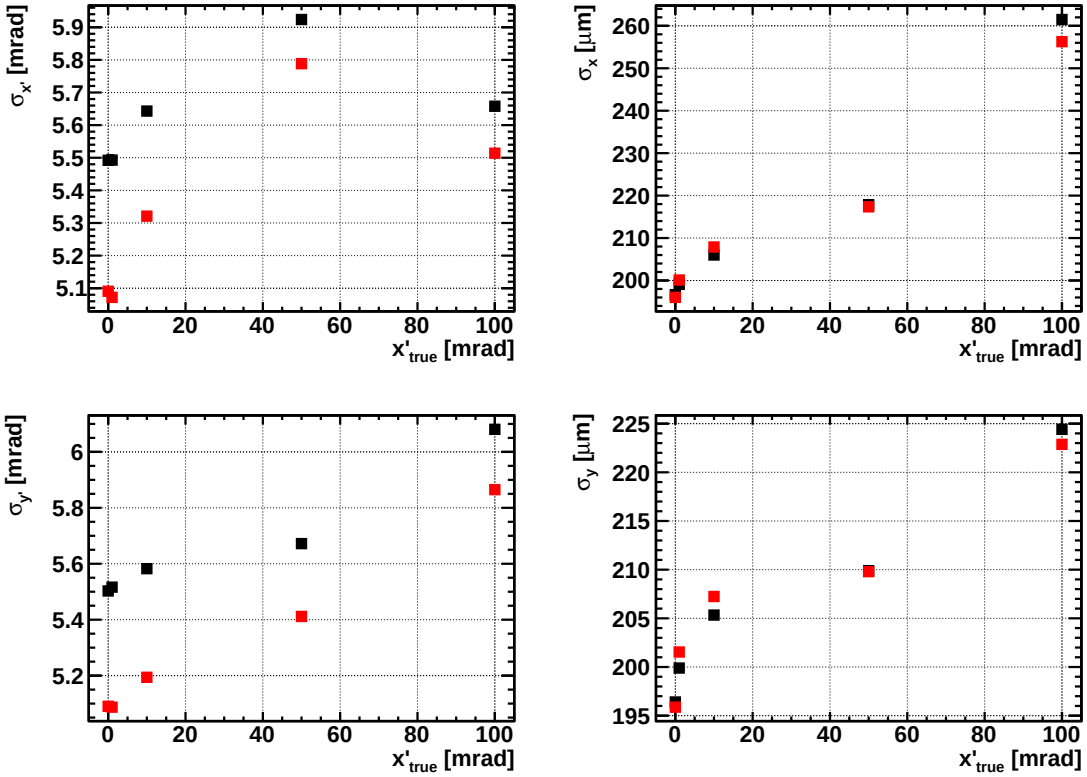

Figure 19: Statistical errors of x', y', x and y as a function of the true x' for an otherwise ideal beam, fitted using only the hit positions (black) and using the deposited energy as well (red). The resolution becomes worse for higher x'.

would be below 100 mrad, the high values were simulated to test the robustness of the fitting algorithm. Like in the ideal beam case, the use of the deposited energy in the fit improves the beam angle reconstruction while having little influence on the position reconstruction. The resolution becomes worse for higher x', but remains stable within a margin of about 50% for x' and y' and about 20% for x and y.

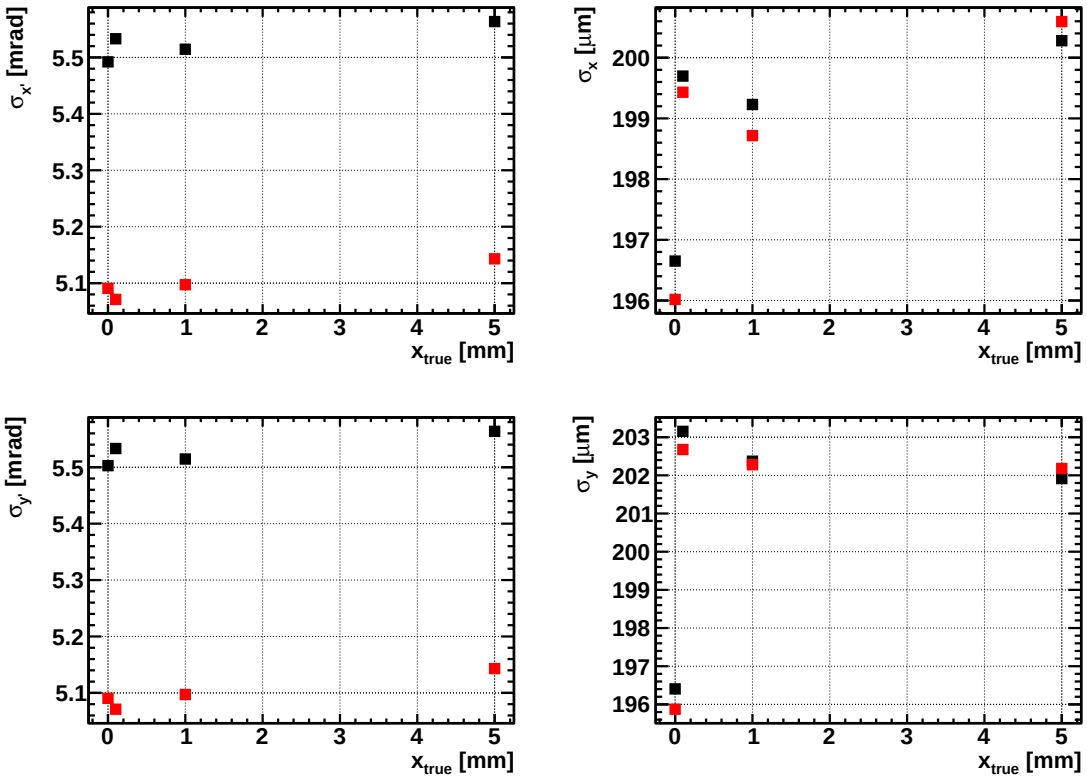

Figure 20: The same as fig. 19 but as a function of the true x. There is no clear trend.

The statistical resolution is stable over a wide range. The fit achieves statistical errors of $5-6$ mrad for x' and y' and $195-205\,\mu$m for x and y. A typical width for a real beam at COSY is in the order of 1 mrad and 1 mm, smaller than the statistical error but in the same order of magnitude. When observing a real beam, the measured distributions would be convolutions of the real distribution and the error distribution. The width of the final distribution would allow conclusions about the true width, although it would not be very accurate. Thus, the fit developed here could in principle measure not only the mean beam position and angle but also its width.

5.3 Systematic Errors

The systematic errors of the beam phase space reconstruction can be studied by applying the method to Monte Carlo data and comparing the results with the known true values. Fig. 21 shows a plot of the reconstructed parameters as a function of the true parameters.

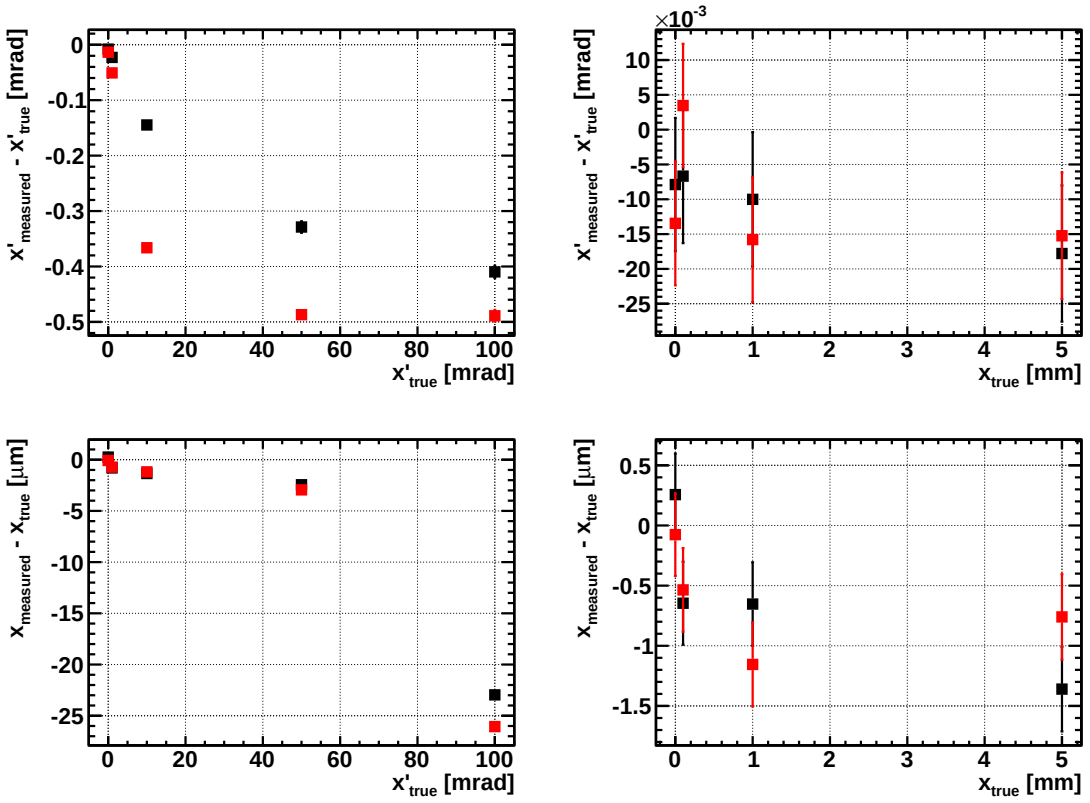

Figure 21: Reconstructed beam parameters as a function of the true values. Each point represents the sample mean and error of one million test events as defined in section 5.2. The black points were fitted using only the hit position information, the red points were fitted using the hit position and the deposited energy.

As in the previous section, each point corresponds to one million test events. The points are the sample mean as defined in the previous section, the error bars denote the statistical error of the sample mean. The plots show a discrepancy between the reconstructed and the true values that cannot be explained by the statistical error alone. In general, the fit tends to underestimate both the beam inclination angle and the distance of the beam from the ideal axis. The systematic errors are greater when the deposited energy

is used in addition to the hit positions. For an ideal beam, the reconstructed values are compatible with the true values. For a beam with a non-ideal x', the reconstructed values differ by 4σ or less from the true values. As all but one of the reconstructed values are smaller than the true ones, this indicates a systematic effect. The fit is much more sensitive to non-ideal x', misalignments here cause discrepancies in the order of 10σ and more.

The main reason for the systematic errors is that the reference histograms were generated for an ideal beam, the difference between the measured beam and the ideal axis is assumed to be small. If x' is positive, particles scattered in positive x-direction hit the detector at a steeper angle and pass less material than for an ideal beam. Hence, they will be scattered less and they will lose less energy. The opposite effect can be observed for particles scattered in negative x-direction.

For a non-ideal beam position, the relation between the spatial resolution of the silicon detectors and the angle resolution for the tracks changes. If the beam is shifted in positive x-direction, particles scattered in positive x-direction will hit the first detector after a shorter distance than particles scattered in negative direction. For the particles scattered in positive x-direction, there are fewer detector strips per solid angle, their track angle will be measured to a worse precision than the angle for particles scattered in negative x-direction. Yet both will be weighted equally. The Monte Carlo uncertainty due to the limited number of events in the reference histograms is not a major source for systematic uncertainties in the reconstruction.

Another important error that could not be studied here is the detector simulation itself. The reference histograms can only be generated with an accurate Monte Carlo simulation. This is especially critical for the deposited energy. While the expected value for the multiple scattering angle is known to be zero and only the shape of the distribution has to be simulated, the mean value for $\Delta E/d$ is also taken from the simulation. The physical processes causing the energy loss are well understood and can be simulated precisely, but the energy calibration and geometry of the detector will have significant uncertainties in a real experiment. The simulated fit using ΔE represents the optimum gain in precision that can be achieved in principle. The results for real applications will inevitably be worse.

The systematic error from the sources that could be simulated can be estimated conservatively at $0.01\,\mathrm{mrad} + 3.5\%$ for x' and y' when using the deposited energy and $0.01\,\mathrm{mrad} + 1.5\%$ when using the hit positions only. The systematic error for x is roughly $1\,\mu\mathrm{m} + 0.25\,\mu\mathrm{m/mrad} \cdot x'$, for y it is $1\,\mu\mathrm{m} + 0.25\,\mu\mathrm{m/mrad} \cdot y'$.

Considering the modest gains in statistical precision achieved by using the deposited energy, using it is probably not worth the additional effort and systematic uncertainty it introduces. As already mentioned, the plots above do not include the uncertainty of the detector calibration, which would make it even less favorable to use ΔE.

5.4 Influence of the Strip Pitch

The simulation was carried out with different values for the strip pitch from 10 to 500 μm. The widths of the resulting distributions were compared to determine the spatial detector resolution required for a satisfying phase space reconstruction. Fig. 22 shows the errors

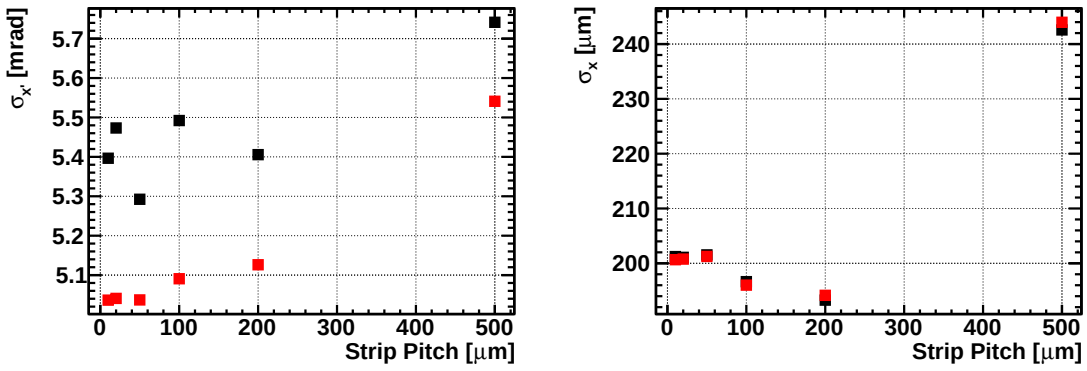

Figure 22: Statistical errors of x and x' for an ideal beam.

of x and x' for an ideal beam as a function of the strip pitch. As the main error for the position measurement comes from multiple scattering, the errors of the fit are not very sensitive to the detector pitch. The error for x' remains almost constant for small strip pitches and only increases noticeably if the pitch is set to 500 μm. The error for x seems to decrease with increasing strip pitch. This is the result of stripe artifacts in the x-y-histogram and does not correspond to a real improvement in precision. Due to the discrete readout of a strip detector, certain discrete values of x and y also appear more often. The histogram has sharp maxima at these points that make the distribution appear sharper. Such artifacts can be seen in fig. 18 for example.

The effect of the strip pitch on systematic errors can be estimated from the plots in fig. 23. The systematic error for the beam angles increases with the strip pitch. The mean beam position increases towards the correct value for increasing strip pitch. Again this is the result of the formation of stripe artifacts. The direction of the trend towards the true value is coincidence.

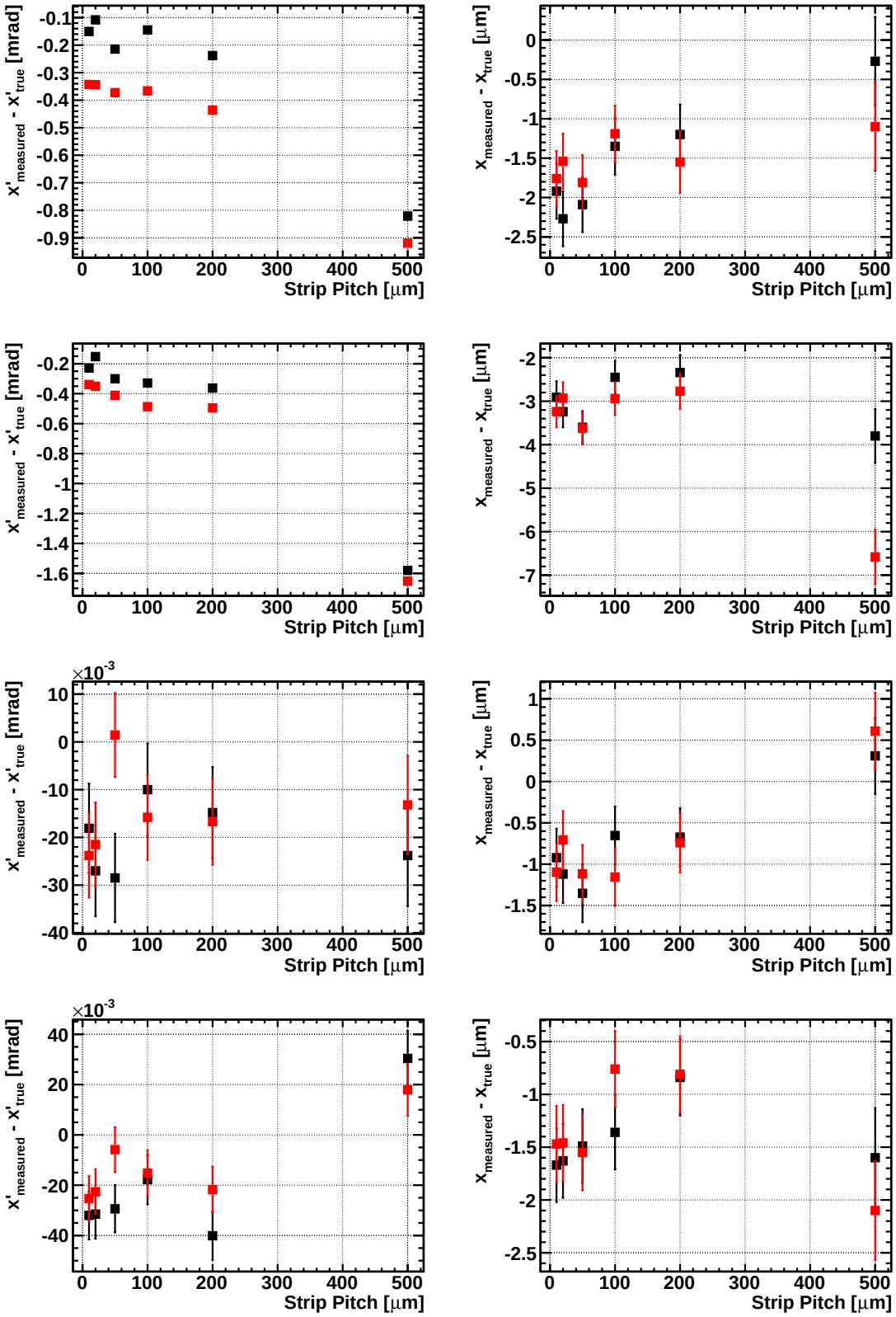

Figure 23: Reconstructed mean x' and x as a function of the strip pitch for beams with $x' = 10\,\text{mrad}$ (first row), $x' = 50\,\text{mrad}$ (second row), $x = 1\,\text{mm}$ (third row) and $x = 5\,\text{mm}$ (fourth row).

5.5 Computational Issues

The fitting procedure does not converge for all points. This is a consequence of the minimization algorithm and cannot be completely avoided. The number of events for which the fit does not converge depends on the beam parameters but is never large, usually staying below $\sim 1\%$ when only the hit positions are used for the fit and around 2.5% when the deposited energy is used as well.

When ΔE is used in the fit, the fit performance depends on the value chosen for the noise suppression threshold (section 4.6), which was set to 10^{-3}, but whose value is somewhat arbitrary. Fig. 24 shows the mean value for x' and the percentage of events

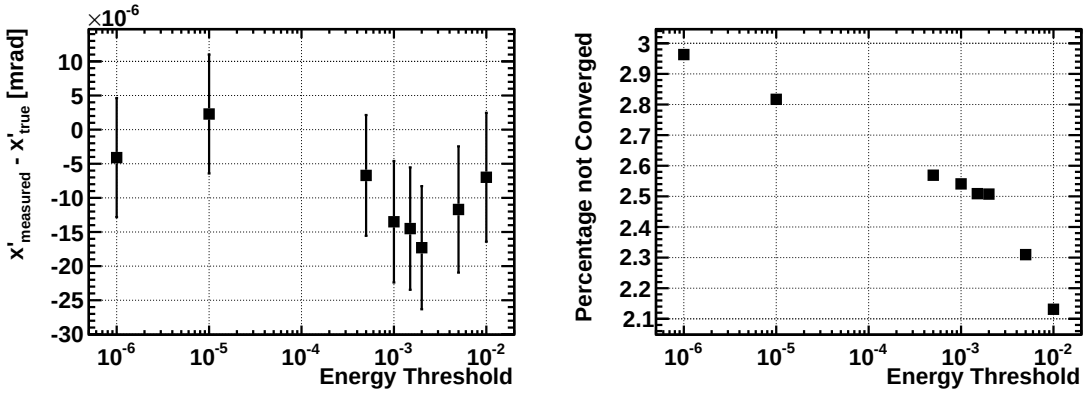

Figure 24: Mean x' and number of events not converged as a function of the energy noise suppression threshold.

that have not converged as a function of the threshold value. There is no clear trend in x', the mean varies by about $2 \cdot 10^{-5}$ mrad. The statistical error increases slightly with increasing thresholds. The effect is in the order of 0.5 mrad for a single event over the range of threshold values in the plot. The number of events that do not converge decreases for higher thresholds. Neither of the plots shows a critical dependence on the threshold, which justifies the choice of 10^{-3}.

It is also noteworthy that the fit creates artifacts in the distribution of the reconstructed θ_{cm} (fig. 25). The fit is more likely to converge at points at which reference histograms were generated. The distribution shows a peak at every such point. This indicates that the interpolation might not be smooth enough so that the original points still stand out from the ones that were interpolated.

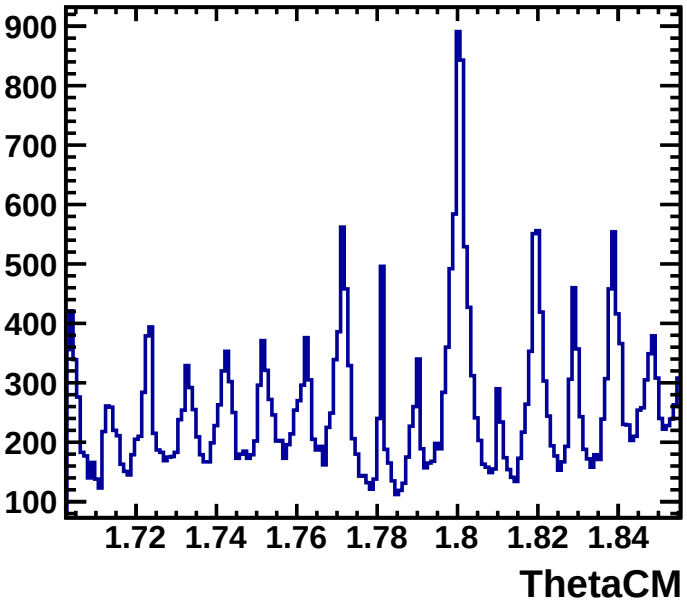

Figure 25: Peaks in the distribution of θ_{cm}. The peaks correspond to the points at which reference histograms were generated.

5.6 Comparison to Beam Position Monitors

Beam position monitors (BPM) are the most widely used instruments to measure the position of a charged particle beam. They are installed in most accelerators including COSY, which uses 31 BPMs. BPMs work by measuring the electrical image charge induced by the beam to determine its position.

BPMs are much simpler than the detector setup used in the simulation and are already present at the storage ring. The detector would mainly serve as a polarimeter, but using it for beam measurements as well would mean higher requirements for the spatial resolution. A polarimeter could be realized by distinguishing only four general directions. Beam measurement using elastic scattering is always destructive while BPMs do not alter the beam.

BPMs are only sensitive to the position (x, y) and not to the beam angle (x', y'). They measure an average position and cannot perform an event by event reconstruction. The angle could only be determined indirectly by measuring the beam position at two points. An additional advantage of beam measurement by elastic scattering is that it can measure the beam as it is at the target. A BPM would have to be installed at some distance.

6 Conclusion

6.1 Results

An algorithm to reconstruct the beam phase space from elastic scattering events was successfully implemented. The concept was tested using a GEANT4 simulation of a detector consisting of two layers of silicon strip detectors situated at a distance of 30.5 and 50.5 mm at each side of the beam. The reaction studied was elastic scattering of deuterons off a stationary proton target at a kinetic energy of 236 MeV.

The transverse momentum and position for each incoming particle could be reconstructed to an accuracy of

$$\sigma_{x',y'} = 5 - 6\,\text{mrad}\ (\text{stat}) + 0.01\,\text{mrad} + 1.5\% \cdot x', y'\ (\text{sys})$$

and

$$\sigma_{x,y} = 195 - 205\,\mu\text{m}\ (\text{stat}) + 1\,\mu\text{m} + 0.25\,\mu\text{m/mrad} \cdot x', y'\ (\text{sys}),$$

where x and y denote the distance of the particle to the detector axis and x' and y' denote the particle's transverse momentum in the respective direction divided by its total momentum. The statistical accuracy is limited by multiple scattering in the inner detector. It was shown that the detector would need a strip pitch of about 100 to 200 μm to work optimally. The accuracy is in the same order of magnitude as the typical width of a beam at COSY (about 1 mm and 1 mrad). The measurement could be sensitive to the angle spread as is would widen the resulting distribution.

The main cause for systematic errors is the assumption of an ideal beam when generating the reference histograms. The simulation computes the likelihood for non-ideal beams semianalytically assuming that the difference from the ideal beam is small. The reconstructed beam parameters are therefore biased towards the ideal beam position.

The phase space reconstruction algorithm can make use of the deposited energy in the detector planes, improving the statistical error of x' and y' by about 0.5 mrad. This requires a precise simulation of the detector response in order to calculate the likelihood of the measured deposited energy as a function of the scattering angle and the beam parameters. The systematic error increases to 0.01 mrad + 3.5% rather than 1.5%. This does not include the uncertainty of the detector simulation, which was not studied. As the energy calibration and geometry of real detectors have significant uncertainties, the results would be worse in a real experiment. The improvement in the statistical error would probably not be worth the additional effort and systematic error.

6.2 Outlook

The beam reconstruction method developed in this thesis does not depend on very specific assumptions on the experiment and could be used for other particle types, energies, and detectors. While the use of the deposited energy only led to modest gains in precision for deuteron-proton elastic scattering, it may prove more helpful in collisions of identical particles, particularly proton-proton scattering at low energies. In these reactions, the opening angle of the tracks only depends on the center of mass scattering angle over relativistic corrections. The scattering angle is therefore more difficult to reconstruct from the hit positions alone.

The fitting algorithm could also be used for different detectors as long as an accurate simulation is available. It could be generalized for detectors with three or more layers or for other types of tracking detectors like scintillating fiber trackers.

References

[1] Dzhygadlo, Kilian, Ritman, Roderburg, Roeder, Sefzick & Wintz (2012). Non-destructive monitoring of proton beam emittance. Verhandlungen der Deutschen Physikalischen Gesellschaft, (Mainz 2012 issue), 1.

[2] D.N. Spergel et al., [WMAP Collaboration], Astrophys. J. Suppl. 148 (2003) 175 astroph/0302209

[3] J. Pretz on behalf of the JEDI collaboration, Measurement of Permanent Electric Dipole Moments of Charged Hadrons in Storage Rings, arXiv:1301.2937v3 [hep-ex]

[4] http://commons.wikimedia.org/wiki/File:NEDM_P%26T_violation.png

[5] D. Fick. Einführung in die Kernphysik mit polarisierten Teilchen. Bibliographisches Institut Mannheim/Wien/Zürich, 1971.

[6] N.P.M. Brantjes et al., Correcting systematic errors in high-sensitivity deuteron polarization measurements. Nuclear Instruments and Methods A 664 (2012) 49-64

[7] G. Ohlsen, P.W. Keaton Jr. Techniques for measurement of spin$\frac{1}{2}$ and spin-1 polarization analyzing tensors. Nuclear Instruments and Methods 109 (1973) 41-59

[8] R. Maier, Cooler Synchrotron COSY - performance and perspectives. Nuclear Instruments and Methods A 390 (1997) 1-8

[9] D. Prasuhn et al., Status of the Cooler Synchrotron COSY Juelich, Proceedings of the 2001 Particle Accelerator Conference, Chicago

[10] S. Sjue, http://skisickness.com/2010/04/25/, accessed July 2014

[11] P. Maanen, RWTH Aachen, III. Physikalisches Institut B. Private Communication (2014)

[12] H. Dombrowski et al., The Münster cluster target for internal storage ring experiments, Nuclear Instruments and Methods A 384 (1997) 228-234

[13] http://geant4.cern.ch/

[14] D. Oellers, Polarizing a Stored Proton Beam by Spin-Flip?, (2010)

[15] http:\\pdg.lbl.gov

[16] F. James, M. Roos, MINUIT — A System for Function Minimization and Analysis of the Parameter Errors and Correlations, Computer Physics Communications 10 (1975) 343 - 367

[17] F. James, MINUIT Tutorial, http://seal.web.cern.ch/seal/documents/minuit/mntutorial.pdf

[18] Maximum-likelihood method. I.A. Ibragimov (originator), Encyclopedia of Mathematics. URL: http://www.encyclopediaofmath.org/index.php?title=Maximum-likelihood_method&oldid=13827

[19] H. Akima, A New Method of Interpolation and Smooth Curve Fitting Based on Local Procedures, Journal of the ACM Volume 17 Issue 4, Oct. 1970

[20] W.H. Press, S.A. Teukolsky, W.T. Vetterling, B.P. Flannery, Numerical Recipes - The Art of Scientific Computing

Selbstständigkeitserklärung

Ich versichere, dass ich die Arbeit selbstständig verfasst und keine anderen als die angegebenen Quellen und Hilfsmittel benutzt sowie Zitate kenntlich gemacht habe.

Unterschrift	Datum